AD-A193 492 INTERFACIAL INFRARED VIBRATIONAL SPECTROSCOPY(U) UTAH 1/1
UNIV SALT LAKE CITY DEPT OF CHEMISTRY S PONS ET AL.
30 JUL 86 TR-63 N00014-83-K-0470

UNCLASSIFIED F/G 7/4 NL

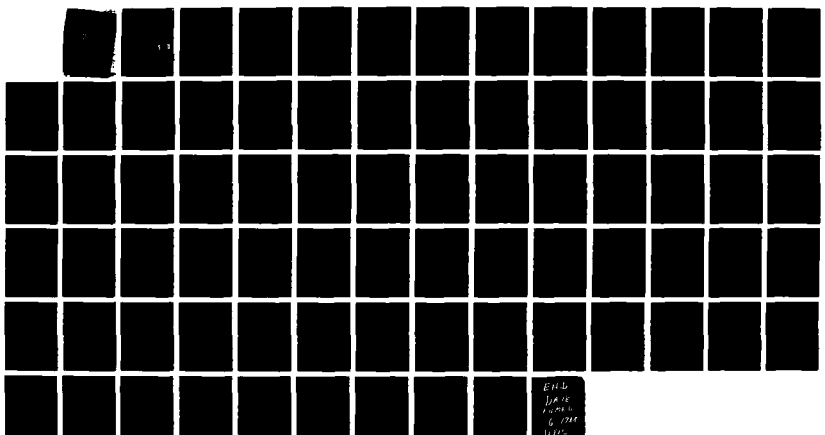

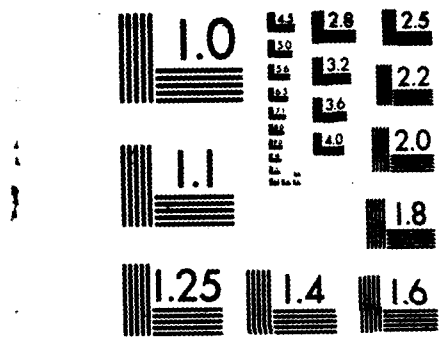

OFFICE OF NAVAL RESEARCH

Contract N00014-83-K-0470-P00003

Task No. NR 359-718

TECHNICAL REPORT # 63

Interfacial Infrared Vibrational Spectroscopy

By

Stanley Pons, J. Foley, J. Russell, M. Seversen

Prepared for Publication in

Modern Aspects of Electrochemistry

University of Utah
Department of Chemistry
Salt Lake City, Utah 84112

July 30, 1986

1. REPORT NUMBER	2. GOVT ACCESSION NO.	3. RECIPIENT'S CATALOG NUMBER

4. TITLE (and Subtitle)	5. TYPE OF REPORT & PERIOD COVERED
Interfacial Infrared Vibrational Spectroscopy	Technical Report # 63
	6. PERFORMING ORG. REPORT NUMBER
7. AUTHOR(s)	8. CONTRACT OR GRANT NUMBER(s)
Stanley Pons, J. Foley, J. Russell, M. Seversen	N00014-83-K-0470-P0003
9. PERFORMING ORGANIZATION NAME AND ADDRESS University of Utah Department of Chemistry Salt Lake City, UT 84112	10. PROGRAM ELEMENT, PROJECT, TASK AREA & WORK UNIT NUMBERS Task No. NR 359-718
11. CONTROLLING OFFICE NAME AND ADDRESS Office of Naval Research Chemistry Program - Chemistry Code 472 Arlington, Virginia 22217	12. REPORT DATE July 30, 1986 13. NUMBER OF PAGES 77
14. MONITORING AGENCY NAME & ADDRESS (if different from Controlling Office)	15. SECURITY CLASS. (of this report) Unclassified 15a. DECLASSIFICATION/DOWNGRADING SCHEDULE

16. DISTRIBUTION STATEMENT (of this Report)

This document has been approved for public release and sale; its distribution unlimited.

17. DISTRIBUTION STATEMENT (of the abstract entered in Block 20, if different from Report)

18. SUPPLEMENTARY NOTES

19. KEY WORDS (Continue on reverse side if necessary and identify by block number)

IR spectroelectrochemistry

20. ABSTRACT (Continue on reverse side if necessary and identify by block number)

A review on (IR) spectroelectrochemistry.

DD FORM 1 JAN 73 1473 EDITION OF 1 NOV 65 IS OBSOLETE

S/N 0102-LF-014-6601

Unclassified

SECURITY CLASSIFICATION OF THIS PAGE (When Data Entered)

Modern Aspects of Electrochemistry, #17
Bockris, Conway, + White, eds.
Plenum Press New York 1986

INTERFACIAL INFRARED VIBRATIONAL SPECTROSCOPY

Stanley Pons* and John K. Foley
Department of Chemistry
University of Utah
Salt Lake City, UT 84112

Joel Russell and Mark Seversen
Department of Chemistry
Oakland University
Rochester, MI 48063

* To whom correspondence should be addressed.

1 INTRODUCTION

The last five years have been to electrochemical infrared spectroscopy what the 1940's were to standard infrared spectroscopy. Prior to World War II, Raman spectroscopy was the most commonly used form of vibrational spectroscopy. The development of infrared technology, particularly detector technology, during World War II led to the rapid growth of infrared spectroscopy. In part due to the relative cost advantage, the use of infrared spectroscopy rapidly overtook Raman spectroscopy for routine vibrational analyses. The advent of the laser produced a resurgence in Raman spectroscopy but it still ranks far behind infrared spectroscopy in routine use. We are today on the verge of a period in which rapid growth in electrochemical infrared spectroscopy can be expected. Furthermore as will be discussed below infrared methods may have greater sensitivity and versatility as a general spectroscopic probe for electrochemical systems than Raman methods. The recent development of electrochemical infrared spectroscopy resulted not from technological breakthroughs but from the marriage of well established electrochemical and spectroscopic techniques.

Electrochemists have recognized the fundamental importance of understanding the chemistry that occurs at the electrode-solution interface. Electrochemical techniques have been developed to easily and precisely control the electrical potential at interfaces thus permitting the investigation of reactions whose energetics span many orders of magnitude. The standard electrochemical techniques do not allow, however, the structure or bonding specificity that may be achieved utilizing vibrational spectroscopic techniques. Early efforts to obtain spectroscopic data for species at the electrode solution interface (1,2,3) utilized infrared transmitting germanium electrodes in an internal reflectance mode. Low sensitivity and restricted

electrode systems limited the utility of the technique. In 1974 Fleischmann, Hendra and McQuillan (4) obtained the first in-situ Raman spectrum for a species adsorbed on an electrode surface. This led to the rapid development of surface enhanced Raman spectroscopy, SERS, (5) and most recently non-enhanced Raman surface spectroscopy (6,7). After hundreds of studies aiming to elucidate the origin of the surface enhancement, studies concentrating on problems of electrochemical importance are appearing.

In 1979 Pons, et. al. (8) showed that the UV/visible specular external reflectance technique which gave useful information for many electrochemical systems (9,10,11,12) could be utilized in the infrared. The ability to discriminate between species at the electrode surface and bulk solution species and the sensitivity necessary to see submonolayer coverages of adsorbates was obtained through modulation of the electrode potential and recovery of the modulated absorbance with phase sensitive detection. Electrochemically modulated infrared spectroscopy utilizing subtractively normalized interfacial FTIR spectroscopy (SNIFTIRS, (13)) and a dispersive spectrometer (EMIRS (14)), have been productively applied to several systems of electrochemical importance. Infrared spectra of species on electrodes have also been obtained using polarization modulation (15,16) with dispersive (17) and Fourier transform spectrometers (18,19). EMIRS and SNIFTIRS spectra are difference spectra for species present at the interface at the two electrode potentials selected as the modulation limits. Polarization modulated infrared reflection absorption spectroscopy, IRRAS, yields spectra for species present at a single electrode potential. All three techniques are sensitive to specific vibrational modes due to an additional surface selection rule in addition to the normal dipole selection rule. Kunimatsu (20) has developed a modification of the EMIRS technique which allows calculation of IRRAS-like

spectra for surface species if an electrode potential is known for which the species is removed from the electrode surface.

These new methods hold great promise for studies in several areas of fundamental and applied electrochemistry, including (i) the identification and reactions of adsorbed and non-adsorbed electrochemical reaction intermediates such as organic ion radicals, (ii) the study of the surface structure, bonding, intermolecular interaction, and dynamics of adsorbates and the effect of electric fields on the parameters, and (iii) the monitoring in various solvent-electrolyte systems of the potential dependent concentrations of molecular and ionic species in the adsorbed state and in the electrical double layer. The specular external reflectance techniques described allow these studies to be made at many types of electrode systems types, including well-defined single crystals, chemically modified surfaces, and semiconductors.

In the subsequent sections of this chapter details of the experimental techniques for EMIRS, SNIFTIRS and IRRAS and applications of these methods will be presented.

1.2 THEORETICAL CONSIDERATIONS AND EXPERIMENTAL TECHNIQUES

1.2.1. Surface Selection Rule

Vibrational spectra of species on or near metal surfaces are subject to a unique surface selection rule due to the physics of reflection of radiation from a highly conducting surface (21). As shown in Fig. 1, s-polarized radiation (electric vector perpendicular to the plane of incidence) at all angles of incidence undergoes a phase shift close to 180°C. P-polarized radiation (electric vector in plane of incidence) has a phase change upon

reflection which varies with the angle of incidence as also shown in Fig. 1. Light reflected from a metal surface combines with the incident light to form a standing wave electric field whose intensity is shown in Fig. 2. The mechanism for absorption of infrared radiation requires a coupling of the electric field with a molecular vibration. Since the intensity of the standing wave electric field parallel to the surface is near zero, only those modes of a species near the metal surface which produce a fluctuation in the dipole moment with component normal to the surface can absorb energy.

These considerations give rise to several important consequences: (1) s-polarized radiation is unable to interact with any dipole at the conducting surface, and thus does not contribute useful information to the spectrum. It is, therefore, usually removed from the beam with an appropriate polarizer before the beam reaches the detector. (ii) Those fundamental vibrations of adsorbed species which do not have a finite value of the dipole derivative (the change in dipole moment with respect to the normal coordinate of the fundamental mode being considered) perpendicular to the surface are unable to undergo interaction with the radiation since there is no mechanism for the generation at the conducting surface of a tangential electric field. The magnitude of the absorbance due to the observable modes will depend on the square of the cosine of the angle of incidence. The relative intensities of bands from the normal mode intensities enable information regarding the orientation of the molecule at the surface to be deduced. (iii) It is indicated, from the above discussion, that p-polarized radiation is able to interact with all species in the optical path; s-polarized radiation is blind to species very close to the electrode surface. The difference between the two beams is simply the absorbance due to molecules located at (or at least near since the low tangential field may extend some distance into the

solution) the electrode surface, all ambient effects having been cancelled out in the subtraction. This latter point has been instrumental in the development of the polarization modulation techniques.

Using this surface selection rule, orientations of species relative to the electrode surface can be deduced from spectra in favorable cases. Care must be exercised in application of the surface selection rule to draw conclusions concerning orientations of surface species. The observation of a vibrational mode such as a C≡O stretch does not in itself prove that the CO molecule is not adsorbed parallel to the surface. As shown in Fig. 3a atoms of the metal surface would produce a surface normal component in the dipole derivative for the stretching mode for CO adsorbed parallel to the surface. This conceivably can allow coupling of the mode with p-polarized radiation. Modes whose dipole derivatives are zero for isolated molecules such as the stretching mode of N_2 would similarly have a *nonzero surface normal* dipole derivative when their symmetry is reduced by interaction with surface atoms. Since the intensity of infrared bands is proportional to the square of the dipole derivative, comparisons of relative intensities of corresponding vibrational modes of adsorbed species may allow use of the surface selection rule for determining orientations of species with respect to the surface. For example the infrared band for CO is expected to be stronger for the perpendicular orientation shown in Fig. 3 than for the parallel orientation.

1.2.2. The Spectroelectrochemical Cell

Cells used for the infrared experiments have been variations of the basic three-electrode, thin-layer cell shown in Fig. 4. A thin-layer cell is required to offset the effects of using strong infrared absorbing solvents such as water. The working electrode, usually consisting of a 5-10 mm

diameter metal disk mounted on a syringe plunger or rod, is polished mechanically or chemically to a mirror surface and positioned at appropriate distances from the cell window. For aqueous solutions window electrode separations of a few microns permit sufficient energy to exit the cell for spectra of surface species to be detected. For nonaqueous solutions larger window-electrode separations are possible. This is particularly useful when one wishes to study electrochemically generated species such as radicals in solution in the thin-layer region. Electrodes are either sealed on glass extensions to syringe plungers or mounted on brass rods covered with Kel-F sleeves machined to mate with the syringe barrel forming the back of the cell. Electrical contact with the solution for most experiments is made only by the front surface.

Various infrared transparent windows have been used. Choice of window material for a particular experiment depends chiefly on the solvent. Windows must be sufficiently insoluble in the solvent of interest and should have a refractive index which permits radiation to strike the electrode at high angles of incidence. Fig. 2 shows that E_p is maximized for angles of incidence near 80°. For aqueous acid solutions the largest angle of incidence possible using a CaF_2 window is near 65°. Higher angles of incidence result in total internal reflection of the beam at the solution-window interface. Cells are easily designed which have prismatic windows to allow normal incidence at the air-window interfaces which minimizes reflection losses. Other materials which have been used for cell windows incude silica, silicon, IRTRAN 2, IRTRAN 4, and zinc selenide. These materials have higher refractive indices than CaF_2 and thus produce lower angles of incidence at the electrode surface. Silica is transparent at wavenumbers above 2300 cm^{-1}. Silicon, although very insoluble and transparent throughout the infrared, is not

transparent in the visible region thus preventing visual alignment of the beam on the working electrode.

The cell design shown in Fig. 4 prevents compensation for electrolyte resistance in the thin-layer thereby giving a relatively long time response. For typical experiments using 1 M aqueous electrolyte a time constant of the order of 5 milliseconds is obtained as the product of the uncompensated resistance and the electrode capacity. Consideration must be made for such longer response times than found for normal cells when designing experiments and interpreting results. When using dilute electrolytes or when the electrochemistry requires sustained currents rather than transient charging currents during the modulation periods, the design of the working electrode may need to be modified. For such experiments an electrode with many small holes drilled through the face and modified so that the rear of the disk is in contact with the solution gives a much faster response and gives a greatly increased area of electrode which is available for species to undergo reaction or adsorption under conditions of greatly reduced uncompensated resistance.

The cell body is also outfitted with a Luggin capillary arrangement for the reference electrode, which is placed so that the tip is about 1 mm from the edge of the working electrode mirror. A wire secondary electrode loop, usually platinum, is mounted internally so that the working electrode cylinder fits through it when inserted. Gas inlet and outlet ports are inserted into the cell for appropriate purging or chemical insertion. A typical reflection setup for the sample chamber is shown in Figure 5. This particular apparatus is used in an FTIR spectrometer.

1.2.3. SNIFTIRS Technique

SNIFTIRS (22) is the difference spectroelectrochemical experiment carried

out on a Fourier transform infrared spectrometer. In its basic form, signal-to-noise is increased by utilization of the multiplex advantage inherent in the modern FTIR instruments. The interferogram, which contains the encoded optical spectrum across the entire instrumentally allowed spectral region, is recorded typically in a few tens to hundreds of milliseconds. Signal averaging of this rapidly acquired data in the first approximation improves the signal-to-noise ratio as the square root of the total number of interferograms collected. Instead of obtaining the difference spectrum between two potential limits with phase sensitive detection as in the EMIRS experiment, the spectra of the interfacial region at each potential are collected separately, and then processed with the instrument computer. Practically, there seems to be almost an even tradeoff between the time necessary to obtain equivalent results with the two techniques. In the case of EMIRS, due to the use of a phase sensitive detector, there is very high discrimination of the signal against noise at each measurement point and, in addition, the infrared detector is operating at the narrow spectral bandwidth defined by the width of the exit slit which optimizes its operating detectivity; these benefits are obtained at the cost of slow acquisition times. For SNIFTIRS the multiplex advantage leads to very rapid acquisition times but there is relatively low discrimination per scan.

The ultimate sensitivity of the FTIR-based technique depends on many factors. The natural form of the interferogram itself puts extreme demands on the electronic design of the instrument. The center burst, which contains only a small portion of the total encoded information, has a very large intensity compared to the rest of the signal. This value sets one of the limits of the A/D converter at a high value, so that the rest of the signal is digitized with poorer magnitude resolution. Although this problem is

mitigated by some software based gain-ranging techniques, it can only be effectively treated by the use of higher resolution A/D converters. The problem of low resolution in the low amplitude wings of the interferograms is particular acute in electrochemical applications since there are usually regions of very high absorbance in the spectrum due to the large effects of solvent and electrolyte. This means that the encoded information in the interferogram corresponding to the surface spectrum will be of very small amplitude; if the interferograms are not sufficiently resolved in the digitization process, this information may be lost. In addition, the problem is exacerbated by the fact that normally the spectrometers are designed to record interferograms using a very large optical bandwidth (for instance 4500 to 400 cm^{-1} with a conventional TGS detector and germanium coated cesium bromide beamsplitter). This leads to a very large amplitude center burst and therefore demands a greater dynamic range than would be the case if a narrower spectral range were recorded. Thus when optical filters can be used to exclude part of the available optical bandwidth without eliminating regions of interest, the digitized information will lead to more accurate transformed data. Sensitivity is thus increased and acquisition time reduced. The use of optical filters has another particular advantage: decreasing the total optical bandwidth at a solid state detector naturally increases its detectivity. If attention is paid to all of these variables, then it is possible to attain near theoretical values of sensitivity; i.e., that governed by the ultimate resolution of the A/D converter.

Spectral resolution is inversely related to the distance which the mirror travels, and directly related to the number of data points per unit time recorded. Although one of the major advantages of the FTIR spectrometer is its ultimate spectral resolution (0.1 cm^{-1} is a typical value), data

acquisition rates are greatly enhanced by working at lower resolutions (see EMIRS section) such a 4 cm^{-1}.

Again, the total energy throughput of any spectrometer will affect its ultimate sensitivity. High intensity sources are always desirable, and careful optical design is critical. The size of the optical beam at the focus in the sample compartment should match as closely as possible the size of the working electrode so as neither to waste energy nor to undersample the electrode surface.

There are several ways to accumulate the data. It has been found that in general the most efficient method is to acquire small numbers of interferograms during tne period that the potential is held at each value and to coadd the new results to previously stored data at each of those potentials. An alternative, acquiring at a given potential for long periods, has a number of disadvantages. First, electronic and mechanical drift over long periods of time are not efficiently cancelled. Second, elimination of any atmospheric absorbances (primarily water and carbon dioxide) is much more difficult: short-time changes are easily cancelled in the subtraction process. Third, in some electrochemical systems, substantial accumulation of products produced by following chemical reactions in the optical cell thin layer may be produced. This can have complicating effects on the spectroscopy: (a) electroactive material is removed over the course of the experiment, which results in the decrease of the measured difference signal. (b) in some cases the products are insoluble which affects the reflectivity in an adverse way. Fourth, we have found that free radicals and other reactive intermediates formed in some reactions, if allowed to accumulate, will attack some optical window materials, which will affect the transmission of the cell and in some cases inject new absorbing species into the optical path.

Treatment of the data is straightforward. From the averaged interferograms at each potential, it is necessary to subtract a blank interferogram of the cell with the electrode withdrawn from the window such that only reflection from the atmosphere/window and window/solution interfaces are recorded. The resulting corrected interferograms may then be ratioed and $\frac{R_1(\bar{\nu})}{R_2(\bar{\nu})} - 1$ calculated, which is equivalent to $\frac{\Delta R}{R}(\bar{\nu})$, the desired quantity. Here, the $R_i(\bar{\nu})$ correspond to the reflectances at each potential.

1.2.4. EMIRS Technique

The fundamental principle underlying EMIRS is use of ac modulation of the electrode potential between two selected values which define two distinct states of the electrochemical system. Thus the chemistry to be observed is directly modulated and may be detected by an appropriate form of synchronous detection. Synchronous detection permits discrimination between absorptions from species modulated by the electrode potential and absorptions from all other species in the ambient electrolyte and all other parts of the total optical path. Sensitivity levels for EMIRS allow detection of changes in absorbance of adsorbates of as small as 10^{-6} of the total signal. With dispersive monochromators modulation rates of 10-1000 Hz are much faster than the wavelength scanning rate thus permitting a phase sensitive detection system with electronic analog smoothing to be used.

The instrument used is a modified dispersive spectrometer with fore-optics for the EMIRS experiment. This instrument and its standard operating procedures have been described in detail (23). The instrument was designed

for high energy throughput with f/3.5 optics. Its source is a Nernst filament operated at about 2300°C. This above standard Nernst temperature reduces source lifetimes to a few weeks but increases the energy output. A polarizer is used to eliminate s-polarized radiation which contains no useful spectral information. The spectrometer may be used with room temperature pneumatic Golay detectors or liquid nitrogen cooled InSb (photovoltaic) and HgCdTe (photoconductive) detectors.

Although the electrochemical modulation technique effectively converts the single beam spectrometer into a near perfect double beam instrument, one beam corresponding to the time interval defined by one half period of the modulation and the second beam to the other half period, the subtraction of the very sharp bands from atmospheric CO_2 and water vapor is considerably enhanced by purging with dry nitrogen. The optimum sensitivity level of 10^{-6} in the measurment of fractional change in reflectivity, $\Delta R/R$, is achieved in high energy regions of the spectrum by accumulating data from many repeated spectral scans. The mechanical chopper is used to modulate the total radiation and determine the reflectivity, R, needed to form $\Delta R/R$ which is directly proportional to the absorbance produced by modulation of the electrode potential. It is possible to simultaneously modulate the electrode potential and total radiation using well separated modulation frequencies. With two lock-in amplifiers tuned to the two modulation rates ΔR and R can be simultaneously measured thus further reducing effects in changes in atmospheric absorption by CO_2 or water vapor.

For dispersive instruments with phase sensitive detection there is a much higher signal to noise ratio for each individual scan than that found in Fourier transform instruments. Furthermore, the narrow spectral bandwidth passed by the exit slit optimizes the operating sensitivity of the detector.

These characteristics of high signal to noise discrimination per scan with slow scans for dispersive instruments and low signal to noise discrimination per scan for very rapid scans for Fourier transform instruments do not clearly favor use of one or the other type of instrument for electrochemical systems. Further details concerning the application of Fourier transform interferometer spectrometers to electrochemical studies have been given (22).

1.2.5. Form of the Spectra

The possible forms that SNIFTIRS and EMIRS difference spectra can possess have been described in detail (23). The origins for features observed in EMIRS spectra can be classified into three groups which produce very distinct spectral characteristics. Featureless shifts in the baseline are attributed to the electroreflectance effect. This effect results from a change in dielectric function of the electrode producing a difference in reflectivity of the electrode at the two potentials defining the modulation limits.

Normal appearing infrared absorption bands may result from a change in the number of absorbing species which may be in solution or adsorbed on the electrode or in the electrical double layer. Such bands may protrude up or down from the baseline depending upon whether there is a larger number of absorbing species at the more negative or more positive potential respectively. Normal single-sided absorption bands could also result from a change in oscillator strength with change in electrode potential. If adsorption/desorption of an absorbing species occurs as the electrode potential is modulated, a band of one sign may be produced by the adsorbed species and at a slightly shifted frequency a band of the other sign produced by a greater number of absorbing species in the solution region.

Bipolar bands would result from changes in band positions or band shapes

as the electrode potential changes even at constant coverage of adsorbed species. The strength of chemical bonds of adsorbed species will generally change with a change in the electrode potential thus producing a change in infrared band position.

It was pointed out during discussion of the surface selection rule that adsorption of species on electrode surfaces will usually reduce the symmetry of the species. Examples were shown in Fig. 3 where an infrared forbidden band such as the N ≡ N stretching mode would be allowed by both the dipole and surface selection rules for parallel and perpendicularly oriented molecules. Parallel oriented CO in Fig. 3 would be surface selection rule allowed due to electrode surface atoms producing a surface normal component to $d\mu/dQ$.

In addition for SNIFTIRS and EMIRS spectra, there is another mechanism which could impart a surface normal component to $d\mu/dQ$ for vibrational modes that would normally be surface selection rule forbidden. It has been well established that infrared spectra of certain charge transfer complexes show large intensity enhancements for some dipole forbidden modes. This enhancement has been attributed to an "electron vibration" mechanism (24) in which the amount of charge transferred from donor to acceptor changes during molecular vibrations. With this electron-vibration model the direction of the dipole moment change can be perpendicular to the direction of motion of nuclei involved in the vibration. A molecule with a π electron system adsorbed parallel to an electrode surface could exhibit the electron-vibration effect made visible to EMIRS by a further dependence upon the electrode potential.

A broader description of this phenomenon is provided by considering the electrochemically activated Stark effect (25). Molecules are always distorted in the presence of external electric or magnetic fields. The most common results are changes in the polarizability and dipole moment of the molecule

which must lead to changes in the optical spectra. Intense electric fields (> 10^4 V cm^{-1}) imposed on gaseous oscillators result in the well-known Q-branch/Stark splitting of the levels (26), as well as the lesser investigated phenomenon of frequency shifting of condensed state vibrational modes (27). In addition, induced dipole moments in these molecules will lead to infrared absorbances that vary quadratically with the external field intensity. The induced dipole moment in a molecule in the direction ℓ of the polarized radiation in a field of strength E_ℓ in the same direction, is given by

$$P_\ell = \alpha_\ell E_\ell$$

where α_ℓ is the value of the polarizability in the direction ℓ. The absorption coefficient is given by

$$B = \frac{2\pi^2 \nu T}{\epsilon_0 hc} |P_{fi}|^2$$

where ν is the optical frequency of the infrared transition, h is Planck's constant, c is the velocity of light in a vacuum, T is the number of absorbing dipoles per unit cross sectional area, ϵ_0 is the permittivity of free space, and P_{fi} is the transition dipole matrix element. The transition dipole matrix element in the presence of an external field is given by (25)

$$|P_{fi}| = |\langle \psi_{\nu_f} | \frac{\partial P_0}{\partial Q} | \psi_{\nu_i} \rangle + E \langle \psi_{\nu_f} | \frac{\partial \alpha}{\partial Q} | \psi_{\nu_i} \rangle|^2$$

where P_0 is the value of the permanent dipole moment. Thus B is calculable from the former equation when the changes in dipole moment and polarizability

with respect to the normal coordinate are known. Upper bound values of B for several electrode-adsorbed systems, as a function of the externally applied field strength, have been tabulated (25).

Electric field strengths across the electrical double layer should be sufficient to induce significant dipole moments in oscillators adsorbed on the metal electrode. As a result, shifts in the frequencies of the normal vibration, infrared activation of modes normally only Raman active, and quadratic electric field dependence of the band intensities are expected. The electrochemically activated Stark effect (TEASE) has been observed and is discussed for specific systems in later sections. Molecules with permanent dipole moments may have induced dipole moments in some modes which will be small compared to the normal dipole moment change. In such cases (CO and ethylene, A_g modes) the induced dipole change may not lead to detectable changes in the observed absorbance. *Highly polarizable* symmetric modes in larger molecules (e.g., naphthalene, anthracene, TCNE, TCNQ) will give rise to large changes in the induced dipole moment and are readily observed (25).

In addition upon adsorption, a molecular species loses translational and some of its rotational degrees of freedom. These lost modes are replaced by new surface vibrational modes. The resulting complex is composed always of reduced symmetry elements. An inversion center is not possible in the overall complex, and neither is a mirror plane unless it contains the surface normal. Thus symmetry elements that can remain are the rotation axes and mirror planes which are normal to the binding surface. Intensities of any new bands arising from the new symmetry will depend on the strength of surface bonding which led to the reduction in symmetry. This will, in general, determine which new bands are indeed observable. Considerations of the possible orientations that a molecule can assume on a well defined surface,

along with the possible two dimensional lattice participating in the binding can lead to a wealth of information regarding the structure and surface orientation of adsorbed species.

A further possibility for complication in the interpretation of SNIFTIRS, EMIRS, and IRRAS spectra results from the possibility that interaction of adsorbates with surface atoms of the electrode may distort the structure of the adsorbate from its free state equilibrium structure. One interesting example of distortion of the molecule itself has been presented by Margrave, et. al. (28). This work describes the interaction of water with metal atom clusters in solid matrices. Infrared spectra of $M\text{-}OH_2$ complexes indicate interaction via electron donation from the σ lone pair orbital (29) of water and not the π lone pair orbital, resulting in a distortion of water toward a linear configuration. Such results may be compared with interactions of water with the metal electrode surface in order to provide information regarding the structure of water in the electrical double layer.

1.2.6. Polarization Modulated IRRAS Technique

Polarization modulated infrared reflection-absorption spectroscopy (IRRAS) takes advantage of the fact that light polarized parallel to the plane of incidence at the metal surface is absorbed much more strongly by adsorbate molecules than that polarized perpendicular to that plane, as discussed above (21). Modulating between the two polarizations results in the intensities of the parallel and perpendicular components of the radiation, I_p and I_s, being alternately detected. This produces an ac signal at the output of the detector which is proportional to $I_p - I_s$. Since I_p is absorbed by surface molecules and I_s is not, the signal includes the infrared spectrum of the adsorbate. Actually, it has been shown (32) that the difference in absorption

between I_p and I_s is obtained within a few microns of the metal surface, which is roughly the thickness of the thin layer of solution used in these experiments. Therefore the ac output signal represents the IR spectrum of the adsorbate and of much of the solution in the thin layer as well.

A number of approaches have been taken to apply this technique to the study of molecules adsorbed on metal surfaces from the gas phase (15,16,30) and in electrochemical systems (17). We shall describe those that have been used for electrode surfaces in solution. These have used a photoelastic modulator (PEM) incorporated into a dispersive (15,17) or an FTIR spectrometer (18,31). In both cases a double modulation scheme has been used which produced both the sum $(I_p + I_s)$ and the difference $(I_p - I_s)$ of the two intensities. Since I_p and I_s are attenuated equally throughout the optical path, except close to the electrode, forming the ratio $(I_p - I_s)/(I_p + I_s)$ allows cancellation of the wavelength dependence of source output, detector response etc., and of absorption by solution species well away from the electrode and of absorption by gas-phase species; this ratio is the infrared spectrum only of species on, and close to the surface. In contrast to SNIFTIRS and EMIRS, the IRRAS spectrum appears as a normal single-sided infrared spectrum and can be obtained at a single electrode potential. However, since absorption by even the few microns of solution seen in an IRRAS experiment is much larger than absorption by surface species, it is usual to take the difference between IRRAS spectra recorded at two potentials in order to subtract out the contributions from solvent and electrolyte.

The principle of operation of the photoelastic modulator is well established (33) and PEMS for the infrared are commercially available (34). The PEM is a transparent cubic crystal which has an isotropic index of refraction when unstressed. A periodic strain is induced into one axis of the

crystal, which results in a periodically changing refractive index for radiation polarized in that direction and hence a periodic phase retardation for radiation with that polarization. In order to produce modulation of I_p and I_s, the stress axis of the PEM is mounted at an angle of 45° with respect to the surface normal, and a fixed polarizer is placed after the PEM with its passing axis either parallel or perpendicular to the plane of incidence. Since both I_p and I_s have components in the direction of the stress axis, the effect of the modulation is to cause both the parallel and perpendicular electric vectors to fall alternately into coincidence with the passing axis of the fixed polarizer and hence be transmitted to the detector.

In dispersive IRRAS (15) the double modulation is effected by using a rotating blade chopper to chop the infrared radiation at a frequency f_c thus modulating the total radiation ($I_p + I_s$), while the difference signal ($I_p - I_s$) is modulated by the PEM/fixed polarizer combination at a frequency $2f_m$, where f_m is the frequency at which the PEM is driven. The PEM is set to modulate the phase retardation between $+\pi$ and $-\pi$ radians at a frequency f_m, and since a retardation of $+\pi$ radians has the same effect as $-\pi$ radians, the intensity difference is modulated at a frequency $2f_m$. Although the maximum phase retardation of $+\pi$ radians is set for a single wavelength, this produces useful modulation of ($I_p - I_s$) for a relatively broad range about the maximum retardation wavelength, as discussed in reference 22. The double modulation produces intensity difference signals at both $2f_m$ and $2f_m \pm f_c$; either of these may be used with the appropriate demodulation scheme.

In the Fourier Transform IRRAS experiment (31) a PEM/fixed polarizer combination is placed in the optical path of the spectrometer. The signal, when treated in the normal way by the signal processing electronics, contains the single beam interferogram of the sample plus spectrometer and is

proportional to $(I_p + I_s)$. There is also a signal at $2f_m$ which when demodulated with a lock-in amplifier results in an interferogram which is proportional to the intensity difference $(I_p - I_s)$. An analog switch is used to allow alternate sampling of the sum and difference interferograms during the same interferometer mirror scan. The two interferograms are Fourier transformed separately and digitally ratioed to produce a spectrum whose amplitude is proportional to $(I_p - I_s)/(I_p + I_s)$.

2.1 APPLICATIONS

Thus far, infrared spectroscopy has been used to investigate a relatively small number of electrochemical problems. The marriage of electrochemical techniques with infrared spectroscopy is a particularly fruitful one, as it allows one to obtain structure-specific information at the electrode-solution interface. In addition, in an electrochemical system one controls the electrode potential, and this means that one can alter the adsorbate-surface and adsorbate-adsorbate interactions in a way not possible in studies of adsorption to surfaces from the gas phase. In the following sections we shall briefly review applications of the infrared techniques to the study of electrocatalytic reactions, molecular adsorption, the detection and identification of ion radicals, and the adsorption of ions at metal surfaces.

2.1.1. ELECTROCATALYTIC OXIDATION/REDUCTION REACTIONS

A complete understanding of the mechanistic pathways for electrocatalytic reactions requires knowledge of the structure and orientations of adsorbed molecules and molecular fragments together with an understanding of the nature of their bonding to the surface and their interactions with other adsorbates and solution species. Despite their structure-insensitive nature, traditional

methods of electrochemistry have enabled considerable progress to be made in some of these areas. However, the new structure-sensitive spectroscopic techniques now provide a direct test for the validity of the structural inferences based on the indirect evidence provided by standard electrochemical measurements and they also may allow additional conclusions to be made concerning bonding and interactions. Since many electrocatalytic reactions are dominated by strong adsorbate/adsorbent interactions in which the solvent plays a relatively minor role, comparisons of electrochemical spectroscopic results with metal/UHV spectroscopic results may be useful. In a number of important cases species which form particularly strong bonds with the metal surface will poison the reaction. These poisons should be easily identified by the spectroelectrochemical methods.

2.2.2. Hydrogen Adsorption from Aqueous Acidic Solution on Pt and Rh

The first interpretations of EMIRS data to propose a model for the orientation and identity of surface species were made from studies of hydrogen adsorption on Pt (35) and Rh (36). These studies suggested that when the Pt or Rh surface is covered with hydrogen atoms in a layer above the surface with each hydrogen bonded to a single metal surface atom the hydrogen atoms are themselves connected via hydrogen bonds to water dimers in the adjacent layer. This conclusion was based upon the observation and relative intensities of vibrational fundamentals, overtones, and combination bands for H_2O, D_2O and HDO.

Hydrogen atoms are known to adsorb on these metals in different sites. The model for adsorbed hydrogen described above in on-top sites is associated

with the first kind of hydrogen to desorb as the potential is made positive from the potential for hydrogen evolution. Another kind of adsorbed hydrogen which is not oxidized off the surface until the potential is made even more positive is thought to consist of a proton buried inside the metal surface with its electron in the conduction band of the metal. When the potential limits for the EMIRS experiment are chosen such that this strongly adsorbed hydrogen is adsorbed and desorbed each modulation cycle, no water bands are observed. This observation is consistent with the buried proton model in which the structure of water in the surface layer does not change during the potential modulation.

We refer here to the potential region between that for oxidation of strongly adsorbed hydrogen and oxidation of the metal as the double layer region. Modulation of the potential between two limits both in the double layer region produces a small featureless shift in baseline attributed to the electroreflectance effect. If the same magnitude modulation width is used but the more negative potential is in the region for strongly adsorbed hydrogen, the shift in baseline is much larger. This larger change in the reflectivity of the metal is consistent with the buried proton model with its associated increase in the number of conduction electrons upon hydrogen adsorption.

2.2.3. Electrocatalytic Oxidation of CH_3OH, HCHO, and HCOOH

Numerous studies of the electrocatalytic oxidation of simple organic molecules (37,38) using standard electrochemical techniques have shown that in acidic solutions active metal electrodes are rapidly inactivated by the

formation of a strongly adsorbed poison. Coulometric evidence has been interpreted to suggest a :CHO species occupying three surface sites as the dominant poison formed during oxidation of many simple organic molecules. Although :CHO appears to be the most widely accepted candidate for the poison in such reactions, the alternative of a $(CO)_{ads}$ poison has been proposed (39,40,41,42).

The described spectroelectrochemical methods offer the ability to identify specific adsorbed species through observation of their vibrational spectra. Such is indeed the case for the identification of the dominant poison for the electrocatalytic oxidation of these organic molecules. The second successful EMIRS study (following the hydrogen adsorption study) and the first IRRAS application to an electrochemical system involved this subject. Systems investigated by EMIRS include methanol on Pt (43), formic acid on Pt, Rh, and Pd (44,45), and formaldehyde on Pt, Rh, and Pd (46). The IRRAS method has been used to confirm the conclusions of EMIRS studies (15,18) as did the optical-electrochemical linear potential sweep method (20). These studies have firmly established a series of $(CO)_{ads}$ species as the strongly adsorbed poisons from the oxidation of each of these molecules on all three metals with one exception: electrochemical measurements have shown that no strong poison is formed during the oxidation of formic acid on Pd.

Three distinct $(CO)_{ads}$ species can be identified from the spectral frequencies at which the CO stretching mode is observed. There is a CO stretch near 2100 cm^{-1} indicating a perpendicularly adsorbed molecule sitting on top of a single metal atom, a band near 1900 cm^{-1} with CO in a bridged site between two surface atoms, and an 1850 cm^{-1} band with CO in a site with strong interaction with three surface atoms is well established from studies on the metal/gas interface (47). The frequency at which each $(CO)_{ads}$ species absorbs

was shown in the metal/gas interface measurements to increase as the surface coverage increased. Electrochemical spectral measurements show this coverage effect as well as a frequency dependence on the electrode potential and the nature of the metal. The number of observed $(CO)_{ads}$ species and their relative populations depend on the coverage and upon the history of the electrode. The EMIRS spectrum of an aqueous acidic solution containing 0.1 M HCHO using a Rh electrode is shown in Fig. 6. Bipolar bands with zero crossings at 1905 cm^{-1} and 2020 cm^{-1} are assigned to $(CO)_{ads}$ species in bridged and linear sites respectively. This spectrum indicates that on Rh the CO bond is strengthened (vibrational band shifts to higher wavenumber) as the electrode potential becomes more positive, but that the amount of each adsorbed species does not change appreciably over the 0.05 V to 0.45 V (NHE) range. Two bands from $(CO)_{ads}$ species are also observed in the oxidation of methanol on a Pt electrode. The shape of the bipolar band for the linear adsorbed species might indicate more adsorbate at the more positive potential due to the stronger negative peak. However, care must be exercised in analyzing shapes of difference spectra since one cannot assume the infrared bands at either potential are symmetric. The appearance of a positive only band for $(CO)_{ads}$ in a three-fold site strongly suggests the conversion of three-fold $(CO)_{ads}$ to linear $(CO)_{ads}$ as the potential becomes more positive.

Identification of the $(CO)_{ads}$ species was confirmed by EMIRS studies of the direct adsorption of CO from solution onto Pt, Rh and Au electrodes (48) and onto a Pd electrode (49,50). IRRAS spectra for aqueous acidic solutions saturated with CO, Fig. 7a, show the shift of the vibrational band with potential. Fig. 7 also compares the difference spectrum formed from subtraction of two of the IRRAS spectra from Figure 7a corresponding to the potentials used as modulation limits for an EMIRS spectrum. The subtracted

IRRAS spectra are shown in Figure 7b and the corresponding EMIRS spectrum in Fig. 7c. In aqueous acidic solutions the shift with electrode potential for the CO stretching mode for linear $(CO)_{ads}$ is to higher wavenumber at a rate of 30 cm^{-1} V^{-1} as the potential is made more positive.

A particularly interesting example of the influence of coverage on $(CO)_{ads}$ species is shown in the spectra for the CO/Pd system, Fig. 8. At low coverage, $\theta < 0.41$, a bipolar EMIRS band is observed in the range for three-coordinate $(CO)_{ads}$. Between $\theta = 0.41$, Fig. 8d, and $\theta = 0.42$, Fig. 8e, there is a sharp increase in intensity and a shift of the bipolar band to a position corresponding to a bridge species. Fig. 9 compares the wavenumber of the observed $(CO)_{ads}$ band vs θ through the region of the reordering phase transition with that observed for the adsorption from the gas phase of CO on Pd(111) (51). The adsorption in the electrochemical case requires the simultaneous desorption of water and bisulfate ions and appears to be sharper. As the total coverage of $(CO)_{ads}$ species increases a band for the linear species appears but even for the highest coverage measured, $\theta = 0.64$, the bridge species remains the dominant one.

Many EMIRS and IRRAS spectra for the direct adsorption of CO on Pt show only linearly bonded $(CO)_{ads}$. A study of the reduction of CO_2 on Pt (52) has established some of the conditions for observation of the various $(CO)_{ads}$ species. Figure 10 shows spectra obtained for a 1M H_2SO_4 solution saturated with CO_2 using various potential modulation limits. No adsorbed CO species are observed when both potential modulation limits lie outside of the hydrogen region, Fig. 10a. With the same modulation width but with one modulation potential in the hydrogen region, Fig. 10c, both three-coordinated and linear $(CO)_{ads}$ species are observed. These spectra indicate that the reduction of CO_2 to $(CO)_{ads}$ takes place by reaction with adsorbed hydrogen. Three-

coordinate $(CO)_{ads}$ appears to form more readily via CO_2 reduction than from direct electrosorption of CO, HCOOH or HCHO under conditions which exclude the formation of CO_2.

The poisoning of the electrode surface in these systems can be at least partially inhibited by the deposition onto the electrode surface of submonolayer quantities of lead (53). Fig. 11 shows EMIRS spectra for the HCHO/Pt system for two potential modulation ranges in the absence (Fig. 11a) and presence (Fig. 11b) of lead (54,55). The shift of the linear $(CO)_{ads}$ band toward lower wavenumbers and its reduced intensity indicate a reduction in coverage of this species in the presence of lead. Failure to observed three-coordinated $(CO)_{ads}$ in Fig. 11b suggests lead atoms are even more effective in blocking these sites.

No EMIRS or IRRAS results have provided any spectroscopic evidence for the presence of an adsorbed COH species. In fact the linear $(CO)_{ads}$ species is stable to very negative potentials even in an HCOOH/Pt system. Even with the forcing conditions of potentials to -0.700 V there is no evidence of the reduction of CO to COH. The close correlation between CO species adsorbed from solution and CO species adsorbed from the gas phase onto metal surfaces prepared in UHV where there is no source of hydrogen rules out the possibility that one of the bands assigned to a $(CO)_{ads}$ species was COH. It must be concluded, therefore, that the hitherto generally accepted preference for the role of COH as the major poisoning species for the electrocatalytic oxidation of these simple organic systems is no longer tenable.

2.2.4. Interactions of $(CO)_{ads}$ with Metal Electrodes, Other $(CO)_{ads}$ Molecules, and Solution Species

The adsorption of CO from the gas phase onto catalytically active metals has been extensively studied by infrared reflectance spectroscopy due to the importance of this system and the intense strength of the infrared absorption of CO. The close similarity between the $(CO)_{ads}$ species formed, either directly or indirectly, on metal electrodes and the comparable species observed on the same metals following adsorption from the gas phase has already been noted. A shift of the CO stretching mode of gaseous CO, 2143 cm^{-1}, to 2064 cm^{-1} for isolated CO molecules adsorbed on a Pt surface is generally attributed to a weakening of the CO bond by the back donation of electron density from a filled Pt d orbital to a π^* CO orbital (56,57). As the coverage of $(CO)_{ads}$ on Pt increases, the CO vibrational bands shifts to a maximum value of 2110 cm^{-1} for the saturated surface. Two mechanisms for the coverage dependence have been proposed. One is a through-space dipole-dipole coupling mechanism (58,59) and the other involves the metal surface (60). Attempts to distinguish these mechanisms have centered on studies of isotopically mixed samples adsorbed on Pt (61).

Electrochemical spectral measurements appear ideally suited to probe the origin of the CO/CO coupling mechanism since the electrode potential can be used to "fine tune" the electronic properties of an electrode surface. The well known linear correlations between the electronegativity of a metal and its work function and between the work function and the potential of zero charge imply that the electronegativity of the atoms in an electrode surface will depend upon the value of the electrode potential. The shift of the vibrational band of linear $(CO)_{ads}$ with potential, $d\nu/dE = 30\ cm^{-1}\ V^{-1}$ for

aqueous acidic solutions, noted in the previous section, can be attributed to a reduction in availability of surface electrons for back-bonding into the π^* CO orbital as the electrode potential is made more positive.

Electrochemical spectral studies permit independent determinations of the effects of changing the electrode potential at constant coverage and of changing coverage at constant potential. In addition both coverage and potential effects can be determined for various isotopic mixtures. Fig. 12 shows EMIRS spectra for various mixtures of $^{12}CO/^{13}CO$ all at saturation surface coverage and the same potential modulation limits. The appearance of a single bipolar band for all isotopic mixtures is an example of extreme intensity stealing by the higher energy vibrational modes of a strongly coupled system of $(CO)_{ads}$ molecules. Fig. 13 shows low and high coverage EMIRS spectra for three $^{12}CO/^{13}CO$ ratios. Other spectra using the same potential modulation width as in Fig. 13 but different modulation limits have similar shapes and intensities but different band positions. Thus variation of electrode potential at constant coverage changes only the position of the CO band but variation of coverage at constant potential changes position, shape and intensity of the CO band. It therefore appears most probable that the primary origins for $(d\bar{\nu}/dE)_\theta$ and $(d\bar{\nu}/d\theta)_E$ for CO/Pt systems are different. The d-π^* back-bonding mechanism believed responsible for $(d\bar{\nu}/dE)_\theta$ acts primarily through a variation of the principle force constant, f_i. The coupling mechanisms suggested to explain $(d\bar{\nu}/d\theta)_E$ could alter the interaction force constant, f_{ij}, alone (as in through-space, dipole-dipole coupling) or alter both f_i and f_{ij} (as in through-metal vibrational coupling). Model calculations for an array of coupled oscillators (62) using a model similar to that used by Moskovitz and Hulse (60) appear to better fit observed EMIRS results such as those in Fig. 13 if the entire coverage dependence is

2.5.2. Adsorption of Bisulfate Ion

In experiments in which aqueous sulphuric acid has been used as the electrolyte, bands in the 900 to 1250 cm^{-1} region are often observed, and these can be assigned to vibrations of the bisulphate ion. These bands are usually not present when other species, such as CO or HCOOH, are strongly adsorbed. EMIRS spectra for 1 M H_2SO_4 on a gold electrode are shown in Fig. 36 (82,54). These show a negative-going band, which is a strong function of electrode potential, superimposed on a broad positive-going background. The broad positive band is thought to be due to changes in absorption of HSO_4^- in solution; hydrogen bonding in the aqueous solution can account for the broadening and overlapping of several bands expected for the bisulphate ion in this region. The negative band has been assigned to increased adsorption of HSO_4^- at the more positive potential. At high potentials, a band assigned to the S-OH stretch, at 950 cm^{-1}, is seen, as well as a band assigned to the SO-H stretch, near 3400 cm^{-1}. These results have been shown to be consistent with rather weak adsorption at the lower potentials, with the ion predominately bound through a single oxygen atom. As the potential becomes more positive, binding through first two, and then three oxygen atoms becomes the most common orientation, and this well defined final orientation is thought to give rise to the strong, sharp band at 1200 cm^{-1} seen at high potentials.

2.5.3 Thiocyanate ion

EMIRS spectra due to adlayers formed from SCN^- on both Au and Pt electrodes have been reported (83). A number of groups have studied the SERS spectrum of SCN^- on Ag (84). Spectra obtained from an aqueous solution of 1 M NaF and 0.01 M KSCN and a Pt electrode are shown in Fig. 37, and show a positive-going band at about 2060 cm^{-1} and superimposed on this a sharp,

negative-going band at 2110 cm^{-1}. In the spectra of S-bonded metal-thiocyanate complexes the C - N stretching frequency appears between 2100 and 2130 cm^{-1}, and by analogy with these results, the 2110 cm^{-1} band has been assigned to adsorbed SCN^-, bonded through the sulfur atom. The lower-frequency, positive-going band is thought to be due to there being less SCN^- free in solution in the thin layer at the more positive potential. At the most positive potential, where anodic oxidation of the anion occurs, the spectra show the disappearance of the adsorbed SCN^- and a large depletion of the SCN^- in solution. The C - N stretching frequency of the adsorbed SCN^- increases as the potential is made more positive; this effect has also been observed for SCN^- on Ag, using SERS (86). The conclusion drawn from the SERS results was that the major species formed on Ag is S-bonded adsorbed SCN^-.

The spectra of an adsorbate formed from thiocyanate ion on gold show more complex behavior and this has been interpreted as involving both N-bonded and S-bonded adsorption of SCN^- (83). These spectra are shown in Fig. 38 for which the electrolyte was aqueous 1 M Na_2SO_4 + 0.005 M KSCN. A small amplitude bipolar band is observed even at the most negative potentials. A partial coverage of S-bonded adsorbed SCN^- could produce this feature if the frequency shift with potential of the C-N stretch is positive as observed for this adsorbate on Pt. A unipolar band at 2060 cm^{-1} appears at +0.2 V, and its intensity increases with increasing potential until at +0.75 $\Delta R/R$ is greater than 4×10^{-3}. The intensity of the bipolar band also increases, but by a much smaller amount. As for SCN^- on Pt, the band at 2060 cm^{-1} could be due to a depletion of SCN^- in solution, but if the solution species is being depleted because of an increased coverage of adsorbed, S-bonded SCN^-, the intensity of the band near 2100 cm^{-1} should increase more than is observed. Another possibility is that both SCN^- in solution and adsorbed, N-bonded SCN^-

contribute to the 2060 cm^{-1} band. In N-bonded metal-thiocyanate complexes, the difference in the C - N stretching frequency between the complex and SCN^- in solution is usually very small, but the intensity of the band in the complex is significantly larger. If this is the same in adsorbed, N-bonded SCN^-, then the desorption of even a small amount of this adsorbate would result in a high intensity positive-going band at 2060 cm^{-1}. This explanation implies that the N-bonded and S-bonded adsorbates are both present at the more negative potentials, and that the coverage of the former decreases and that of the latter increases at potentials greater than +0.1 V. The fact that only the S-bonded species contributes to the spectrum at more negative potentials could result from the value of $d\bar{\nu}/dE$ for the C - N stretch in N-bonded SCN^- being very small. The very small change in the C - N stretching frequency on going from free SCN^- to the N-bonded species may be consistent with this. These results provide evidence for both N-bonded and S-bonded SCN^- adsorbed on Au, but further experiments are required to verify the existence of both these species.

2.5.4 Cyanide ion

There have been two reports of the infrared spectrum of adsorbed cyanide, on Au and Ag using EMIRS (85), and on Ag using IRRAS (19). The SERS spectrum for CN^- on Ag has been studied extensively (86-97). The IRRAS study showed a band at 2080 cm^{-1} with frequency and intensity independent of electrode potential, and another band at about 2100 cm^{-1}, which shifted to higher wavenumber and increased in intensity as the potential was made more positive. The 2080 cm^{-1} band was assigned to the C - N stretch of cyanide ion in solution, and the potential-dependent band near 2100 cm^{-1} to an adsorbed cyanide species. The results of the EMIRS study (85) were similar; for Ag

they show a single bipolar band near 2100 cm^{-1}, and its potential dependence showed that $d\bar{\nu}/dE$ for the absorption band giving rise to this feature is about 30 cm^{-1}/V, the same as observed with IRRAS. Since the shift with potential was the same as that observed for CO on Pt, and since CN^- is isoelectronic with CO, this was felt to be evidence that the mechanism for the band shift with potential was the same for the two adsorbates, and that CN^-, like CO, is bound in a linear configuration on Ag (26). Another possibility is that the adsorbate is a surface complex such as $Ag(CN)_2^-$ (85).

IRRAS measurements made at more positive potentials at which oxidation of the electrode begins showed a decrease in intensity of both the 2080 and 2100 cm^{-1} bands, and the growth of a new band at 2136 cm^{-1}. Since this band could be observed with both s- and p-polarized light alone, it was concluded that it was due to a solution species, and was assigned to $Ag(CN)_2^-$ (19).

A comparison of the infrared results discussed above with the previously reported SERS results (86-97) shows that the peak position and dependence on potential of the band due to the surface cyanide species are similar in both experiments, although the line width observed in the Raman spectra is much larger than that observed with IRRAS. None of the SERS spectra show bands due to the solution species that are observed with IRRAS. Comparison of infrared measurements of vibrational spectra of adsorbates with SERS measurements may help in understanding the origin of the SERS effect.

2.5.6. Hexacyanoferrate

The ferro/ferricyanide redox couple in aqueous solutions has been used for many years as a model for the study of heterogeneous electron transfer reactions. The electron transfer is thought to take place by an outer sphere mechanism, with quasi-reversible kinetics (the rate constant is around 10^{-2}

cm s^{-1} at room temperature). Recent reports, however, have suggested that the reaction is not as simple as has been supposed. Observations have included the marked dependance of the electron transfer rate constant on the composition of the supporting electrolyte (98,99) and the possible adsorption of the complex ions at the electrode (100,101). There is evidence in the latter paper for adsorption of the ions through a -CN group bonded via the nitrogen atom to the surface platinum atoms.

The system has been investigated with the SNIFTIRS technique in the C ≡ N stretching region of the spectrum (102). Figure 39 shows the difference spectra of ferrocyanide oxidation as a function of potential modulation using, instead of the usual square wave potential program a staircase potential program. Here one hundred interferograms are co-added at each potential, and each set of data is normalized to $\Delta R/R$ by dividing by a previously stored set of data taken at the -0.20 V base potential. The solution contained 5 mM $K_4Fe(CN)_6$ with 0.50 M K_2SO_4 as supporting electrolyte. The band directed upward at 2040 cm^{-1} is due to depletion of the bulk $Fe(CN)_6^{4-}$ species as it is oxidised to $Fe(CN)_6^{3-}$ at the more positive potentials. This band increases in intensity with increasing positive potential, until a constant intensity is reached when all the $Fe(CN)_6^{4-}$ in the thin layer has reacted. The band directed downward at 2114 cm^{-1} is due to formation of $Fe(CN)_6^{3-}$ at the more positive potential. The intensity of this band also increases with potential, reaching a maximum value at a slightly lower potential (+0.25 V) than the potential at which the $Fe(CN)_6^{4-}$ band has its maximum (+0.30 V). However, this band decreases in intensity with further increase in potential, indicating a loss of some of the $Fe(CN)_6^{3-}$ species at high positive potentials. Electronic spectroscopy of solutions of $K_3Fe(CN)_6$ under these same conditions indicate that the $Fe(CN)_6^{3-}$ species is stable in bulk

solution. The disappearance of $Fe(CN)_6^{3-}$ can be most easily explained by adsorption onto the electrode at very positive potentials. There are two other bands in the spectrum, a peak at 2092 cm^{-1} and a shoulder at 2061 cm^{-1}. The 2092 cm^{-1} band shifts in frequency with potential (by -100 cm^{-1}/V) and its intensity varies with potential in the opposite manner to the intensity of the 2114 cm^{-1} $Fe(CN)_6^{3-}$ band. The 2092 cm^{-1} band can therefore be assigned to the adsorption product of $Fe(CN)_6^{3-}$. The shoulder at 2061 cm^{-1} is at the same wavelength as adsorbed CN^- (this refers to a separate experiment in which previously adsorbed CN^- was displaced from the electrode by SO_4^{2-} as the potential was stepped from -0.20 V to +0.40 V). This band is evidence for surface decomposition of $Fe(CN)_6^{3-}$ upon adsorption.

The same experiment was performed on a solution containing $K_3Fe(CN)_6$ as the substrate instead of $K_4Fe(CN)_6$ (Figure 40). In this case, the base potential, to which the spectra were normalized to give $\Delta R/R$ values, was +0.4 V. At this potential adsorbed $Fe(CN)_6^{3-}$ must be present. The band at 2114 cm^{-1}, corresponding to loss of $Fe(CN)_6^{3-}$ at the more negative potential, approaches a maximum intensity and remains constant. The $Fe(CN)_6^{4-}$ band at 2040 cm^{-1}, corresponding to production of that species, does the same. There is no evidence for the production of a new adsorbed species following the reduction of $Fe(CN)_6^{3-}$, nor desorption of the adsorbed species discussed above. This experiment suggests that the adsorption of $Fe(CN)_6^{3-}$ at high positive potentials is irreversible.

Further evidence for the irreversibility of the adsorption is provided by data from the difference spectra as a function of potential modulation using the usual pulse technique. With other experimental conditions the same as for above (i.e., using the substrate $K_4Fe(CN)_6$, and a base potential of -0.20 V), only the bands for removal of bulk $Fe(CN)_6^{4-}$ (2040 cm^{-1} and for

attributed to the interaction force constant. This suggests the importance of dipole-dipole coupling although current experiments cannot rule out a minor or even major contribution by through-metal coupling.

The electrochemical spectral results also show a further shift in the CO frequency due to interaction with solution species. Isolated $(CO)_{ads}$ adsorbed on Pt from the gas phase show an infrared band at 2064 cm^{-1} while the corresponding band for CO adsorbed from aqueous acidic solutions occurs at 2030 cm^{-1}. The position of the linear $(CO)_{ads}$ on Pt for saturated surface coverages are 2110 cm^{-1} (gas) and 2080 cm^{-1} (solution). Preliminary results for the CO/Pt system for adsorption from methylene chloride and acetonitrile show that $d\bar{\nu}/dE$ for these solvents are 15 cm^{-1} V^{-1} and 17 cm^{-1} V^{-1} respectively (63). Completion of $^{12}CO/^{13}CO$ and coverage studies in these organic solvents is expected to contribute additional insight into the interactions of $(CO)_{ads}$ species.

2.3.1. MOLECULAR ADSORPTION

Several examples of non-dissociative, molecular adsorption have been investigated. Two such examples will be reviewed. The adsorption of acrylonitrile and benzonitrile on gold provided spectroscopic evidence for orientations of the adsorbates which were contrary to expectations. Adsorption of difluorobenzene gives rise to bands which are predicted by the surface selection rule.

2.3.2. Difluorobenzene Adsorption

The SNIFTIRS investigation of adsorbed benzene derivatives seem to be well described by the surface selection rules (64). Thirteen of the normal vibrational modes of p-difluorobenzene are infrared active. All of these

modes represent dipole changes in the plane of the aromatic ring except for the last three. The b_{3u} modes, each with dipole derivative changes perpendicular to the molecular plane, will be expected to undergo absorption of radiation if the species is adsorbed with the molecular plane parallel to the metal surface ("flat" adsorption). The b_{1u} and b_{2u} modes would not be expected to absorb radiation since their dipole changes all lie in the molecular plane. The converse is true for adsorption of the species with the molecular plane perpendicular to the metal surface ("edge" adsorption). For any intermediate position ("skew" adsorption) all transitions will be expected.

The SNIFTIRS spectrum for p-difluorobenzene (0.5 mM in 1.0M perchloric acid) between the potential limits of 0.200 V (base potential) and 0.400 V vs NHE at a platinum mirror electrode is shown in Figure 14. The bands extending to positive values of $\Delta R/R$ correspond to absorption by the predominant species in the optical path at +0.200 V, the solution dissolved p-difluorobenzene. The bands extending to negative values correspond to the adsorbed species at +0.400 V. It should be pointed out that the total quantity of p-difluorobenzene in the thin layer of solution between the electrode and the optical window is less than that required to form a complete flatly adsorbed monolayer of difluorobenzene. Any solution dissolved p-difluorobenzene that may be present in the thin layer at the higher potential will manifest itself as a decrease in the magnitude of the positive extending bands. It is observed that there are negative bands corresponding to two of the b_{3u} modes normally occurring at 833 and 509 cm^{-1}. Under the present conditions these are shifted to 811 and 495 cm^{-1} respectively. These results strongly suggest that the molecular species is adsorbed on the platinum metal surface in a flat configuration. The red shift in the b_{3u} modes in the adsorbed state is

expected since interaction of the surface with the π-electrons of the aromatic system will tend to decrease the orders of the bonds involved in those modes.

The SNIFTIRS spectra of the meta- and ortho- isomers are shown in Figure 15. These show again that the molecule lies flatly adsorbed at the more positive potential. Negative bands are observed that are associated with each of the normal vibration absorptions which have dipole derivative changes perpendicular to the principal molecular symmetry plane. In no instance is there a corresponding band for adsortion for the fundamentals which are associated with in-plane vibrational modes.

Figure 16 shows the results of an experiment where the potential modulation amplitude is varied. The absorption band pictured corresponds to the b_{3u} C-C-C out-of-plane bending mode. As the potential is increased from the same initial base of 0.200 V to more positive potentials, the negative band corresponding to the adsorbed species is seen to undergo an increasingly larger red shift, in accord with the comments mentioned above. Any such shift with potential is attributed to adsorbed species only. It is noted that the positive band of the solution dissolved species is unaffected by the change in potential as expected. The integrated area under the positive and negative lobes are equal to within experimental accuracy, and it is thought that there is approximately monolayer coverage (64). It is also important to note that even at the highest potential used there is no sign of bands from the b_{1u} and b_{2u} modes. Although, as explained earlier, these are disallowed by the surface reflection rule, they could appear by a mechanism which is essentially a manifestation of the Stark Effect and involves vibronic coupling to the high electrical field at the electrode surface (25). We conclude, therefore, that for the fluorobenzenes the polarizability changes during the b_{1u} and b_{2u} vibrations are too small to lead to observable field effects.

Hubbard and Soriaga (65) have made similar observations for a number of adsorbates in the same electrode/electrolyte system. One paper of their series points to the restructuring of the adsorbed layer when the isothern equilibrium is shifted strongly to the surface by increasing the concentration of the solution dissolved species. The results for an experiment involving the effect of substrate concentration is shown in Figure 17. The potential modulation was from 0.200 to 0.400 V. Again, the electrolyte was perchloric acid, and as in Figure 5, the spectrum represents the b_{3u} C-C-C bending mode. The temperature of the cell was 281 K. Up to concentrations of about 0.5 mM, the entire spectrum is identical to that described above. At solution concentrations above 0.8 mM however, there is a marked increase in the magnitude of the bands and negative bands now appear for all of the modes instead of just the b_{3u} species. We attribute the appearance of these new bands, and the increase in intensity to an increase in surface density of adsorbed species by the forced skewed packing by virtue of the increased solution concentration (65). The b_{1u} and b_{2u} modes are now able to interact with the radiation since the skewed species will have perpendicular dipole derivative components for every fundamental mode.

2.3.3. Orientations of Adsorbed Benzonitrile and Acrylonitrile on Au

The electronic structures of benzonitrile and acrylonitrile offer two possible orientations for these molecules to adsorb onto electrodes. The molecules might adsorb parallel to the electrode surface via bonding by their π electron systems. Such bonding would likely involve σ donation of π-bonding electrons from the molecule to empty orbitals on the metal and π back-bonding of filled metal d orbitals with empty π^* orbitals of the adsorbing

molecule. Both types of bonding would weaken the CN bond shifting the position of the CN stretching mode to lower wavenumbers from its value for solution species. Varying the electrode potential to more positive values would strengthen the σ donation and weaken the d-π^* back-bonding. The former effect would produce a shift toward lower wavenumbers and the latter a shift toward higher wavenumbers as the electrode potential is made more positive. To a first approximation the intensity of the CN stretching mode for parallel oriented benzonitrile and acrylonitrile should be low. Observation of such modes with nuclear displacements parallel to the surface would result from surface normal dipole derivatives resulting from bonding to surface atoms or from a change of the polarizability derivative with respect to the normal mode as discussed above under the surface selection rule.

The other possible orientation for these molecules with respect to the electrode surface is one with the molecular planes normal to the surface and bonding via the N atom. Nitrogen metal bonding would likely involve donation of N lone pair electrons to empty metal orbitals and d-π^* back bonding from filled metal orbitals to empty π^* adsorbate orbitals. Since the nitrogen lone pair orbital is somewhat antibonding (66), donation of lone pair electrons to metal orbitals would strengthen the CN bond and produce a shift toward higher wavenumber for the infrared band. As noted above d-π^* back-bonding has the opposite effect. For both of these bonding mechanisms a shift in electrode potential to more positive values would strengthen the CN bond and shift the infrared band toward higher wavenumbers. Since the CN bond in this orientation is normal to the surface, a strong CN stretch infrared mode is expected.

EMIRS spectra with varying cathodic potential modulation limits for the CN stretching region are shown in Fig. 18 for benzonitrile adsorbed on a gold

electrode in 1 M H_2SO_4. The dominant spectral feature is the negative band which becomes stronger and shifts toward higher wavenumbers as the cathodic limit for the potential modulation is made more positive (until at very positive potentials formation of gold oxide and oxidation of benzonitrile inhibit the adsorption). The sign of the band corresponds to greater absorption at the more positive potential limit. The increase in band intensity with more positive potentials indicates greater adsorption at the more positive potentials. A weak positive single sided band is observed at 2229 cm^{-1}, the position of the CN stretching mode of solution benzonitrile. The sign of this band indicates greater absorption at the more negative potential. This observation is also consistent with removal of solution benzonitrile to form the adsorbed species at the more positive potential. The weak intensity of the solution band relative to the band of the adsorbate is likely due to the averaging over random orientations of the surface normal component of the dipole derivative and the rapid reduction of the effects of potential modulation for species in solution. These spectral features are all consistent with an orientation of the molecular plane perpendicular to the surface with bonding via the nitrogen atom. The appearance of the CN stretching mode for adsorbed benzonitrile at a higher wavenumber than solution benzonitrile implies the dominance of the bonding via the nitrogen lone pair with empty metal orbitals over d-π^* back-bonding. Further evidence for the perpendicular orientation is shown in Fig. 19. Two A_1 benzene ring modes appear in this spectral region and are observed in the EMIRS spectrum as negative bands at 1480 cm^{-1} and 1595 cm^{-1}. Furthermore a weak B_1 mode at 1448 cm^{-1} is observed as a positive band corresponding to a solution species which is depleted as more molecules are adsorbed.

The voltammetry of the gold electrode in sulfuric acid (1 M) over a ten-

fold concentration range of acrylonitrile indicates adsorption of that species (67). This is confirmed by double layer capacitance measurements (Figure 20) which also indicate probable adsorption of bisulfate anion. In general, there is considerable decrease in the capacitance across the entire potential range investigated. There is a sharp rise in capacitance beyond 1V which signifies desorption of the nitrile and onset of oxide formation. Low concentrations of nitrile were used in all experiments to avoid the possibility of polymerization. No evidence (2115 cm^{-1} and 2165 cm^{-1}) appeared for polymerization at these concentrations. It is concluded that across the entire potential range between hydrogen evolution and oxide formation, there is strong adsorption of the nitrile.

Spectroelectrochemical measurements for several potential modulations were carried out over the 1950 cm^{-1} to 2450 cm^{-1} potential range. Two bands at about 2130 cm^{-1} and 1520 cm^{-1} were observed (Figure 21).

The amplitudes and positions of these bands were found to be potential dependent. Excessive noise amplitude on the 1520 cm^{-1} band is due to the low energy throughput in the region of the water bending mode. We note that these two bands correspond to the C ≡ N and C = C stretching modes of adsorbed acrylonitrile if it is assumed that the bands are red shifted about 100 cm^{-1} compared to the frequencies of the free molecule. As pointed out, the frequency shifts would be expected to be smaller (especially the C = C stretch) and in the opposite direction for C ≡ N if the molecule were adsorbed vertically through the nitrogen. Therefore, it is proposed that the molecule lies <u>flat</u> on the electrode which raises other arguments:

(a) Single-sided instead of bipolar bands are observed; changes in frequency at constant surface coverage or changes in coverage with potential would give rise to bipolar bands.

(b) The surface selection rules discussed earlier preclude observing bands that are due to modes which exhibit values of the dipole derivative parallel to the surface.

(c) The C ≡ N is considerably weaker than the adsorbed benzonitrile C ≡ N stretch.

(d) The C = C band is stronger than the C ≡ N band, whereas the opposite situation is true for the free molecule.

Two possible mechanisms can explain the presence of a flatly adsorbed molecule under the influence of a process that produces relatively small unipolar bands:

(a) The symmetry and bonding in the adsorbate/adsorbent complex produces vibrational modes leading to a finite component of the dipole derivative perpendicular to the surface, and

(b) There is vibronic coupling of the high electric field in the double layer to the vibrational motion by virtue of the polarizability tensor.

This latter mechanism is another example of what has been termed the electrochemical Stark effect by Pons, et. al. (25). Figure 22 shows the variation of band intensity with electric field strength near the electrode surface for the 2130 cm^{-1} band. As pointed out in section 1.2.5, the intensity of the band should be proportional to the square of the field magnitude. It is difficult to test this exactly in this system since it is

not known precisely where the field strength is zero, nor what is the exact dependence of the field on the potential applied. It is clear, however, that when the modulation symmetrically spans the zero field point, there must be an inflection maximum in the observed absorption intensity. Such a maximum is observed in Figure 22 near where one would expect the zero field potential.

The detailed line in the figure denotes the square law relation predicted for a simple potential-field relationship (field strength proportional to potential with zero located at E = 0.70 V). Even though this is a crude approximation when considering the large change in double layer capacitance and adsorption of bisulfate (Figure 20), the fit is encouraging support for the Stark explanation. The potential dependence of the band position also deserves comment. Unlike data for other systems such as CN^- on Ag and CO on Pt electrodes, the position is non-linear (Figure 23). The positive slope of the plot indicates surface bonding primarily by electron donation from the metal orbitals to the π^* antibonding level of the organic nitrile. The extent of transfer would be expected to decrease at more positive potentials resulting in an effective increase in the CN bond order. If the bonding was primarily due to donation of electrons to the metal by the π level of the acrylonitrile, the potential dependence would be reversed. This inference is consistent with expected behavior for metals with filled d-orbitals.

The difference between acrylonitrile and benzonitrile in orientation and bonding to the surface is not easy to explain. Acrylonitrile has the greater dipole moment per unit volume and would have the greater tendency to be oriented perpendicular to the surface by the electrical field, whereas the adoption of this orientation by benzonitrile maximizes the interaction between the aqueous solution and the hydrophobic end of the molecule. Molecular orbital calculations on the two molecules (68) do lend support to stronger

bonding between the metal and the nitrogen in the case of benzonitrile. The energy of the lone pair orbital of the nitrogen atom is considerably higher for benzonitrile than for acrylonitrile. If the adsorption is regarded as a soft coordination reaction in which the electron pair of the adsorbate is shared with a vacant orbital of a surface metal atom, as suggested by Barclay, et. al. (72), then bonding via the nitrogen would be stronger for benzonitrile than for acrylonitrile and it would also increase with increasing positive potential, as is observed.

2.3.4. Investigations of Species in the Double Layer

Infrared spectroscopy has been used to study species in the double layer formed at a platinum electrode in acetonitrile solutions (69). Spectra obtained for different potential limits in a solution of 0.1 M tetrabutylammonium tetrafluoroborate (TBAF) which was about 1 micrometer thick are shown in Fig. 24. The reference potential in all cases is -0.5 V vs. Ag/Ag^+ in TBAF in acetonitrile. The spectra show large changes in the 1100 cm^{-1}, 1400 cm^{-1}, 2350 cm^{-1} and 3000 cm^{-1} regions. The solution was estimated to contain less than 10^{-4}M water. The effect of making the solution 0.10 M in water is shown in Fig. 25; these spectra show additional changes in the 1630 and 3200-3700 cm^{-1} regions. Figs. 26 and 27 show spectra obtained under the same conditions for 0.10 M lithium perchlorate in acetonitrile.

The increasing intensity of the band at 2350 cm^{-1} may be explained by increasing adsorption of acetonitrile at the electrode as the potential is increased. Thus the C ≡ N stretching frequency of adsorbed acetonitrile shows a large blue shift from that observed for bulk acetonitrile, 2220 cm^{-1}, indicating strong perturbation of the molecule upon adsorption (70). The strong bands at 1102 cm^{-1} for $LiClO_4$ and 1060 cm^{-1} for TBAF may be assigned to

vibrations of the perchlorate and tetrafluoroborate anions, whose populations in the double layer should increase at high positive potentials.

When water is added to either solution, additional bands result which may be assigned to the vibrations of water molecules in various environments. The broad band at 3350 cm^{-1} corresponds to water which is extensively hydrogen bonded. It may be associated with the anion, as the intensity of the band increases when there is more anion in the double layer at the high positive potentials. The sharper bands at 3625, 3550, and 1625 cm^{-1} appear to be due to water which is not so strongly perturbed by hydrogen bonding. A likely candidate for this species is the symmetrically bonded complex between one water molecule and two acetonitrile molecules. This species has been studied in detail (71,72,73) and has characteristic bands in its infrared spectrum at the wavenumbers listed above. The intensities of these bands decrease at the more positive potentials, indicating a decrease in population for this species.

The behavior of the system may be described in terms of the relative populations of various species in the double layer region. As the electrode potential is made more positive, more anions are present in the double layer to balance the charge, and more acetonitrile is adsorbed at the electrode surface (70), resulting in the increase in the appropriate bands in the vibrational spectrum. Bulk acetonitrile and its associated water are forced out of the region, and there is seen to be less intensity in the bands due to these molecules at the higher positive potentials. Bands are also observed in the C-H stretching region of the spectrum; the direction and potential dependence of these are consistent with their being due to vibrations of the tetrabutylammonium cation, whose population in the double layer should decrease at the more positive potentials.

These experiments demonstrate that the infrared methods may be used to obtain quite detailed information on the composition of the double layer.

2.4.1. ION RADICAL INTERMEDIATES

The infrared spectrum of an organic ion radical may be obtained using the thin layer reflectance cells which have been described above. Solution layer thicknesses of about 50 μm are used, typically and the ion radicals are generated in aprotic solvents by controlled potential electrolysis. Almost all of the organic substrate in the thin layer is converted during the electrolysis, after which several interferograms are collected. If the system electrochemical couple is reversible, then the ion radical is reconverted to the substrate by returning the potential to the rest value; if the system is not reversible, then the thin layer is flushed and replaced with fresh substrate solution forced through the thin layer with argon. In either case, reference spectra are recorded at the rest potential.

2.4.2. Benzophenone

The benzophenone ketyl anion radical was electrogenerated at a potential of -2.50 V vs. Ag/Ag^+ (0.01 M and 0.1 M TBAF in acetonitrile) reference, and the rest potential was -1.75 V. The SNIFTIRS difference spectrum of the system is shown in Fig. 28 (74). In this spectrum, positive-going bands are due to greater absorbance at the rest potential, and negative-going bands are due to greater absorbance at the generation potential. An infrared transmission spectrum of the benzophenone substrate is also shown in Fig. 28 for comparison. As shown in Table 1, the observed spectrum of the ketyl anion radical matches closely with those reported by other workers.

Table 1.

BENZOPHENONE KETYL BANDS (cm^{-1})

This work	Literature (75)
976 (vs)	970 (vs)
1019 (w)	1025 (w)
1143 (vs)	1147 (vs)
1150 (s)	1155 (s)
1260 (vs)	1249 (vs)
1288 (m)	1288 (w)
1398 (w)	1394 (m)
1560 (vs)	1555 (vs)

key: s = strong, m = medium, w = weak; v = very

In the spectrum of Fig. 28, there is a large difference in the wavenumber of the C = O stretching band between the ketyl anion (1555 cm^{-1}) and the substrate (1661 cm^{-1}). This large shift is due to the transferred electron being strongly localized at the C = O moiety. The ring modes show a shift to lower frequency in going from the neutral molecule to the ketyl anion (76). The spectra in the figure were obtained using a very thin solution layer of about 1 μm. These show bands at 1340, 1464, and 2120 cm^{-1} that are not observed with thicker solution cells or conventional spectra of the ketyl anion. The intensities of these bands compared to those from the anion radical in solution and the dependence upon solution thickness indicate tha

they are due to adsorbed intermediates, the most likely of which is a complex between the ketyl anion and adsorbed acetonitrile (77). Further work on this system is in progress.

For a reversible electron transfer reaction, it can be shown that under conditions of semi-infinite linear diffusion, the normalized reflectance should increase linearly with $t^{1/2}$, where t is the electrolysis time. These conditions should hold for the relatively thick solution layer experiments discussed above. Using the rapid scan mode available with most FTIR spectrometers it is possible to obtain interferograms at short time intervals during the duration of the pulses at the generation potential, -2.50 V, and this linear relationship between the normalized reflectance and $t^{1/2}$ was verified for each of the bands recorded. If care is taken that the contents of the thin-layer are reproducibly returned to rest conditions after each pulse to the electrolysis potential, then quantitative time resolved spectrochemistry is possible using this technique.

2.4.3. Anthracene

The anthracene anion radical was generated by electrolyzing a solution of 5 mM anthracene in 0.1 M TBAF in acetonitrile at -2.50 V vs. the Ag/Ag^+ reference, and the rest potential was -1.50 V (78). The difference spectrum for this system is shown in Fig. 29, as is a transmission infrared spectrum of anthracene in a KBr pellet. The fact that only bands due to the anion radical species appear indicates a relatively large difference in the intensities of the bands due to the two species. A careful examination of the individual single beam spectra taken at the two potentials showed that some of the bands are the same in both species, and thus do not appear in the difference spectrum, since of course, the difference spectrum will only display bands

that are not common in both frequency and intensity to both species. Stark activation of some A_g modes is observed under some conditions, (see Section 1.2.5).

2.4.4. Phenylaniline

The cation radical of 2,6-di-t-butyl-4-phenylaniline was generated at +0.8 V vs. the same reference as above (78). The rest potential was 0.0 V, and the resulting difference spectrum is shown in Fig. 30. As before, the spectrum of the cation radical is represented by the negative-going bands in the difference spectrum. The electrode mirror was platinum, the thin layer thickness was 15 μm, and the substrate concentration was 5.0 mM in dry acetonitrile with 0.1 M lithium perchlorate support electrolyte.

2.4.5. Adsorption of Tetracyanoethylene Anion Radical (79)

The cyclic voltammetry for TCNE in acetonitrile solutions containing $LiClO_4$ and tetra-n-butylammonium tetrafluoroborate (TBAF) are shown in Figure 31. The solid trace (TBAF) shows reversible behavior for the formation of the anion radical, followed by a quasi-reversible formation of the dianion. The dashed trace ($LiClO_4$) shows more reversible electron transfer behavior for the second process. The difference in the electrochemical behavior could be explained in several ways: complexation of the anion radical by the TBAF electrolyte, distortion of the TCNE anion, or adsorption of electrolysis products at the interface to the point where further electron transfer to the anion radical is inhibited. It is found that the solubility of the TCNE dianion/electrolyte cation ion pair complex is highly dependent on the structure of the electrolyte. For instance, mixtures of lithium perchlorate and TBAF in a 1:1 mole ratio interact with the dianion and give very sharp

voltammetric adsorption peaks.

Conventional transmission spectra in the C≡N stretch region of the neutral TCNE molecule (KBr, Nujol mull, and solution) and the conventional spectrum of the anion in acetonitrile are shown in Figure 32. The four bands at 2265 cm^{-1} ($\nu_9(B_{1u})$C≡N stretch), 2230 cm^{-1} ($\nu_{15}(B_{2u})$C≡N stretch, 2215 cm^{-1}, and 2203 cm^{-1} are in agreement in frequency and relative magnitude with those for neutral TCNE. The anion radical spectrum (Figure 32d) was made after bulk electrolysis of TCNE substrate in acetonitrile. It is noted that there is a band around 2225 cm^{-1} for the anion in solution, and a broad band at about 2220 cm^{-1} for the neutral TCNE in solution (composed of the 2230 cm^{-1} and 2215 cm^{-1} bands). The SNIFTIRS spectra of the species present very near the interface during a modulation experiment between + 0.5 V and - 0.5 V are shown in Figure 33. By normal convention, bands extending downward ($-\frac{\Delta R}{R}$) are representative of the majority species at the working (E_2) potential (-0.5 V), while those extending upward are indicative of the majority species at the base (E_1) potential (+ 0.5 V).

The spectrum in $LiClO_4$ solution (Figure 33b) is very similar to that reported for the bulk solution soluble anion radical of TCNE: The bands at 2185 cm^{-1}, 1420 cm^{-1}, and 1185 cm^{-1} and 523 cm^{-1} may be assigned to the $\nu_1(A_g)$ C ≡ N symmetric stretch, the $\nu_2(A_g)$ C = C symmetric stretch, the $\nu_{16}(B_{2u})$ C - C, and the $\nu_3(A_g)$ C - C stretch of the anion radical, respectively (80). Infrared activity of the A_g modes is best explained by dimerization of the monoanions in solution, or strong ion pairing to the electrolyte cation, environs necessary for vibronic activation of this normally inactive mode (vide infra). The band at 1456 cm^{-1} is dependent on oxygen content of the solution and is attributed to a decay product of TCNE anion. It was difficult to tell if any of the bands at wavelengths less than

300 cm^{-1} were due to the anion, since the noise level in that region (purged spectrometer instead of vacuum) was high. Use of subtraction routines available on the Brucker instrument indicated that possibility however. The other C≡N anion band at 2225 cm^{-1}, apparent in Figure 32d, is not observed in Figure 33b since it is cancelled by the 2220 cm^{-1} band of the neutral species in the computer subtraction process. The strong band at 2145 cm^{-1} observed for the solution soluble anion has not been reported previously. The 2145 cm^{-1} band is close to that reported (2146 cm^{-1}) (81a) for the $\nu_{15}(B_{2u})$ C≡N stretch of the TCNE dianion. This possibility however, must be rejected for the following reasons. (i) The maximum potential applied to the electrode was 200 mV more positive than the half wave potential of the anion/dianion couple, which implies that even if the pulse time was long enough to attain bulk equilibrium, the maximum dianion concentration could only be about 0.05% of the total TCNE concentration or about 10^{-6} M. (ii) Formation of dianion from disproportionation of anion radical is precluded since the formation constant is on the order of 10^{-10}. (iii) Electrolysis of the solution just past the second voltammetric wave leads to formation of the dianion and a new C≡N stretch at 2120 cm^{-1}, which is probably the $\nu_{15}(B_2u)$ C≡N stretch shifted (by the solvent or ion-ion interactions) from the 2146 cm^{-1} reported for the solid state. The intense positive bands at 1060 cm^{-1} (Figure 33a) and 1100 cm^{-1} (Figure 33b) are due to the increased amount of tetrafluoroborate and perchlorate respectively, in the double layer at the more positive potential (+ 0.5 V).

The spectrum obtained in a TBAF solution in a cell with a 1 μm solution layer is quite different (Figure 33a) from $LiClO_4$ solution. The experiment was performed in the same thin layer cell with the same electrode configuration. The thin layer contained approximately 10^{-9} mol TCNE (about

the amount necessary to form one monolayer coverage if all were adsorbed in a close-packed arrangement on the Pt surface). The weak bands associated with the ν_2 and ν_{16} stretch modes of the anion are now buried in the background noise, and the C≡N bands described above are markedly decreased in intensity. A prominent band has appeared at 2080 cm^{-1}, which is close to that reported for the $\nu_1(A_g)$ C ≡ N symmetric stretch of the Na_2TCNE solid state electron donor/acceptor (EDA) complex (81). In addition, bands at 1475 and 1325 cm^{-1} are now in the spectrum.

Three experiments confirm that these three new bands represent vibrational modes of an adsorbed species. Figure 34 shows the spectral results (in the C≡N region for clarity) as the concentration of substrate TCNE is varied. The bands attributed to the solution soluble species (2145 and 2185 cm^{-1}) increase in integrated intensity as expected, whereas the intensity of the band at 2080 cm^{-1} remains constant. This is the expected result if the electrode is at maximum equilibrium coverage with the adsorbed species at the working potential (-0.5 V). Figure 35 shows the effect of changing the polarization state of the incident radiation at the indicated angle of incidence, and performing the experiment at constant concentration of TCNE substrate. The intensity of the 2080 cm^{-1} band is a function of polarization; the largest absorbance being recorded when the electric field vector is polarized such that it lies in a plane perpendicular to the electrode surface and thus has a component normal to the surface. The 2145 and 2185 cm^{-1} bands (solution soluble species) remain constant in intensity, as is expected. Finally, the three bands being attributed to an adsorbed species have positions which are dependent on the magnitude of the electrode potential. Thus the 2080, 1475, and 1325 cm^{-1} bands exhibit $d\bar{\nu}/dE$ coefficients of +15 ± 4, -30 ± 5, and -10 ± 4 cm^{-1}-V^{-1} respectively.

The above data suggests the following model for the adsorbed TCNE species: TCNE is one of the strongest π electron acceptors known. When the compound forms EDA complexes in the solid state with alkali metals (see 81 and references therein) there are shifts in the infrared bands as the TCNE to metal ratio is changed. Up to four distinct sets of spectra are obtained as the ratio is varied from 1:1 to 1:4. The spectra have been assigned to the anion, dianion, trianion, and tetraanion respectively (81a). As more electrons are added to the TCNE molecule, it is observed that the C≡N and C=C fundamentals shift to lower f.equencies since the lowest unoccupied MO's available are antibonding with respect to those bonds. The π-bond orders for C≡N and C=C decrease from 0.87 and 0.76 to 0.79 and 0.42 respectively in going from the neutral molecule to the dianion. At the same time, the π-bond order for the C-C bond increases from 0.35 to 0.56. It is noted that the C-C bond becomes almost twice as strong as the C=C bond in this progressive addition of electrons. Hemminger (81d) has observed strong interactions between a Ni(III) surface and adsorbed TCNE molecules, and interactions between successively adsorbed TCNE layers on that surface. Red shifting of the C≡N and C=C stretch bands to 2204 cm^{-1} and 1512 cm^{-1} respectively were observed. This behavior has been attributed to the formation of charge transfer complexes (EDA) at the surface with the subsequent donation of electrons to TCNE from the metal surface orbitals which, as in the alkali neutral complexes, results in the strong decrease in bond order of C≡N and C=C. It is reasonable to assume that adsorption of the anion radical onto the Pt electrode would result in the same behavior. The adsorbed TCNE anion, still being a strong π electron acceptor, would continue to exhibit decreasing bond order in the C≡N and C=C moieties, and increasing bond order in the C-C bond as the electron population in the surface is increased (potential made

more negative): the next anion orbitals available for electron transfer are antibonding with respect to the C≡N and C=C bonds, and bonding with respect to the C-C bond. This model also implies that the TCNE anion is adsorbed flat on the electrode; a configuration that could not be observed directly by SNIFTIRS if the surface selection rule is operative; there are no components of the dipole derivative associated with ν_1 or ν_2 that are normal to the electrode surface. It is well known, however, that the TCNE anion polarizability in the infrared is very high, a fact substantiated by its intense visible electronic absorption spectrum. Any external field interacting with the easily polarizable electron will thus induce a vibronic interaction in the anion, affecting its infrared vibrational spectrum. Devlin (81) has pointed out, in a convincing manner, that these effects are quite predominant in TCNE anion, and charge vibration is responsible for the activation of the normally infrared inactive A_g modes of TCNE anion. A strong polarization vector normal to the electrode surface, parallel to the intense (10^8V-cm^{-1}) electric field across the electrical double layer thus could induce the dipole changes necessary to cause interaction with the radiation. A similar explanation has been suggested for the bands observed from acrylonitrile adsorbed flat on a gold electrode (see above). There has been no evidence for a structure whereby the anion is adsorbed standing up on the surface with bonding through the nitrogens of two -C≡N groups on one end of the molecule. This would demand a blue shifting of the -C≡N stretch frequency as well as the appearance of two bands corresponding to the two types (bound and unbound) of -C≡N. Based on the above, assignments are made for the band at 2080 cm^{-1} to the $\nu_1(A_g)$C≡N symmetric stretch, the 1475 cm^{-1} band to the $\nu_2(A_g)$C=C symmetric stretch, and the 1325 cm^{-1} band to the $\nu_{16}(B_{2u})$C-C stretch of flatly adsorbed TCNE$^-$ on polarized Pt electrodes (- 0.5 V vs. the Ag/Ag$^+$ (0.01 M) in

acetonitrile) in the presence of a non-coordinating, non-specifically adsorbed electrolyte (TBAF).

There is one further difficulty which arises from the assumption of flat adsorption. In such a case, vibronic activation of the B_{2u} modes (i.e. the 1325 cm^{-1} band for the adsorbed anion) would not be expected. This difficulty would be overcome, however, if the adsorbed molecule is distorted by the four C ≡ N groups moving slightly out of the plane so that the C = C moiety lifts slightly away from the electrode surface. This distortion could be due to interaction with electrolyte cation located on the solution side of the molecule. This interaction is well substantiated in the electrochemical results mentioned above. We believe this explanation to be more likely than one involving pure edge-on adsorption, which would also enable the B_{2u} modes to be observed, but which suffers from the major disadvantage that it requires two pairs of non-equivalent C ≡ N groups; this would lead to the appearance of additional C ≡ N modes which are not observed.

As mentioned the differences in the two sets of results due to the type of supporting electrolyte is still not fully understood. Since there are no significant differences in the bulk solution vibrational spectra of the anion radical in these two electrolytes, it is assumed that the effect is due to a specific surface interaction which is dependent on the solubility of the electroactive species.

2.5.1. ADSORPTION OF IONS

In many of the applications discussed above, various bands in the infrared spectra have been attributed to adsorbed electrolyte ions. In this section, experiments with a number of ions which are strongly adsorbed on the electrode surface will be discussed in more detail.

2.5.2. Adsorption of Bisulfate Ion

In experiments in which aqueous sulphuric acid has been used as the electrolyte, bands in the 900 to 1250 cm^{-1} region are often observed, and these can be assigned to vibrations of the bisulphate ion. These bands are usually not present when other species, such as CO or HCOOH, are strongly adsorbed. EMIRS spectra for 1 M H_2SO_4 on a gold electrode are shown in Fig. 36 (82,54). These show a negative-going band, which is a strong function of electrode potential, superimposed on a broad positive-going background. The broad positive band is thought to be due to changes in absorption of HSO_4^- in solution; hydrogen bonding in the aqueous solution can account for the broadening and overlapping of several bands expected for the bisulphate ion in this region. The negative band has been assigned to increased adsorption of HSO_4^- at the more positive potential. At high potentials, a band assigned to the S-OH stretch, at 950 cm^{-1}, is seen, as well as a band assigned to the SO-H stretch, near 3400 cm^{-1}. These results have been shown to be consistent with rather weak adsorption at the lower potentials, with the ion predominately bound through a single oxygen atom. As the potential becomes more positive, binding through first two, and then three oxygen atoms becomes the most common orientation, and this well defined final orientation is thought to give rise to the strong, sharp band at 1200 cm^{-1} seen at high potentials.

2.5.3 Thiocyanate ion

EMIRS spectra due to adlayers formed from SCN^- on both Au and Pt electrodes have been reported (83). A number of groups have studied the SERS spectrum of SCN^- on Ag (84). Spectra obtained from an aqueous solution of 1 M NaF and 0.01 M KSCN and a Pt electrode are shown in Fig. 37, and show a positive-going band at about 2060 cm^{-1} and superimposed on this a sharp,

negative-going band at 2110 cm^{-1}. In the spectra of S-bonded metal-thiocyanate complexes the C - N stretching frequency appears between 2100 and 2130 cm^{-1}, and by analogy with these results, the 2110 cm^{-1} band has been assigned to adsorbed SCN^-, bonded through the sulfur atom. The lower-frequency, positive-going band is thought to be due to there being less SCN^- free in solution in the thin layer at the more positive potential. At the most positive potential, where anodic oxidation of the anion occurs, the spectra show the disappearance of the adsorbed SCN^- and a large depletion of the SCN^- in solution. The C - N stretching frequency of the adsorbed SCN^- increases as the potential is made more positive; this effect has also been observed for SCN^- on Ag, using SERS (86). The conclusion drawn from the SERS results was that the major species formed on Ag is S-bonded adsorbed SCN^-.

The spectra of an adsorbate formed from thiocyanate ion on gold show more complex behavior and this has been interpreted as involving both N-bonded and S-bonded adsorption of SCN^- (83). These spectra are shown in Fig. 38 for which the electrolyte was aqueous 1 M Na_2SO_4 + 0.005 M KSCN. A small amplitude bipolar band is observed even at the most negative potentials. A partial coverage of S-bonded adsorbed SCN^- could produce this feature if the frequency shift with potential of the C-N stretch is positive as observed for this adsorbate on Pt. A unipolar band at 2060 cm^{-1} appears at +0.2 V, and its intensity increases with increasing potential until at +0.75 $\Delta R/R$ is greater than 4×10^{-3}. The intensity of the bipolar band also increases, but by a much smaller amount. As for SCN^- on Pt, the band at 2060 cm^{-1} could be due to a depletion of SCN^- in solution, but if the solution species is being depleted because of an increased coverage of adsorbed, S-bonded SCN^-, the intensity of the band near 2100 cm^{-1} should increase more than is observed. Another possibility is that both SCN^- in solution and adsorbed, N-bonded SCN^-

contribute to the 2060 cm^{-1} band. In N-bonded metal-thiocyanate complexes, the difference in the C - N stretching frequency between the complex and SCN^- in solution is usually very small, but the intensity of the band in the complex is significantly larger. If this is the same in adsorbed, N-bonded SCN^-, then the desorption of even a small amount of this adsorbate would result in a high intensity positive-going band at 2060 cm^{-1}. This explanation implies that the N-bonded and S-bonded adsorbates are both present at the more negative potentials, and that the coverage of the former decreases and that of the latter increases at potentials greater than +0.1 V. The fact that only the S-bonded species contributes to the spectrum at more negative potentials could result from the value of $d\bar{\nu}/dE$ for the C - N stretch in N-bonded SCN^- being very small. The very small change in the C - N stretching frequency on going from free SCN^- to the N-bonded species may be consistent with this. These results provide evidence for both N-bonded and S-bonded SCN^- adsorbed on Au, but further experiments are required to verify the existence of both these species.

2.5.4 Cyanide ion

There have been two reports of the infrared spectrum of adsorbed cyanide, on Au and Ag using EMIRS (85), and on Ag using IRRAS (19). The SERS spectrum for CN^- on Ag has been studied extensively (86-97). The IRRAS study showed a band at 2080 cm^{-1} with frequency and intensity independent of electrode potential, and another band at about 2100 cm^{-1}, which shifted to higher wavenumber and increased in intensity as the potential was made more positive. The 2080 cm^{-1} band was assigned to the C - N stretch of cyanide ion in solution, and the potential-dependent band near 2100 cm^{-1} to an adsorbed cyanide species. The results of the EMIRS study (85) were similar; for Ag

they show a single bipolar band near 2100 cm^{-1}, and its potential dependence showed that $d\bar{\nu}/dE$ for the absorption band giving rise to this feature is about 30 cm^{-1}/V, the same as observed with IRRAS. Since the shift with potential was the same as that observed for CO on Pt, and since CN^- is isoelectronic with CO, this was felt to be evidence that the mechanism for the band shift with potential was the same for the two adsorbates, and that CN^-, like CO, is bound in a linear configuration on Ag (26). Another possibility is that the adsorbate is a surface complex such as $Ag(CN)_2^-$ (85).

IRRAS measurements made at more positive potentials at which oxidation of the electrode begins showed a decrease in intensity of both the 2080 and 2100 cm^{-1} bands, and the growth of a new band at 2136 cm^{-1}. Since this band could be observed with both s- and p-polarized light alone, it was concluded that it was due to a solution species, and was assigned to $Ag(CN)_2^-$ (19).

A comparison of the infrared results discussed above with the previously reported SERS results (86-97) shows that the peak position and dependence on potential of the band due to the surface cyanide species are similar in both experiments, although the line width observed in the Raman spectra is much larger than that observed with IRRAS. None of the SERS spectra show bands due to the solution species that are observed with IRRAS. Comparison of infrared measurements of vibrational spectra of adsorbates with SERS measurements may help in understanding the origin of the SERS effect.

2.5.6. Hexacyanoferrate

The ferro/ferricyanide redox couple in aqueous solutions has been used for many years as a model for the study of heterogeneous electron transfer reactions. The electron transfer is thought to take place by an outer sphere mechanism, with quasi-reversible kinetics (the rate constant is around 10^{-2}

cm s^{-1} at room temperature). Recent reports, however, have suggested that the reaction is not as simple as has been supposed. Observations have included the marked dependance of the electron transfer rate constant on the composition of the supporting electrolyte (98,99) and the possible adsorption of the complex ions at the electrode (100,101). There is evidence in the latter paper for adsorption of the ions through a -CN group bonded via the nitrogen atom to the surface platinum atoms.

The system has been investigated with the SNIFTIRS technique in the C ≡ N stretching region of the spectrum (102). Figure 39 shows the difference spectra of ferrocyanide oxidation as a function of potential modulation using, instead of the usual square wave potential program a staircase potential program. Here one hundred interferograms are co-added at each potential, and each set of data is normalized to ΔR/R by dividing by a previously stored set of data taken at the -0.20 V base potential. The solution contained 5 mM $K_4Fe(CN)_6$ with 0.50 M K_2SO_4 as supporting electrolyte. The band directed upward at 2040 cm^{-1} is due to depletion of the bulk $Fe(CN)_6^{4-}$ species as it is oxidised to $Fe(CN)_6^{3-}$ at the more positive potentials. This band increases in intensity with increasing positive potential, until a constant intensity is reached when all the $Fe(CN)_6^{4-}$ in the thin layer has reacted. The band directed downward at 2114 cm^{-1} is due to formation of $Fe(CN)_6^{3-}$ at the more positive potential. The intensity of this band also increases with potential, reaching a maximum value at a slightly lower potential (+0.25 V) than the potential at which the $Fe(CN)_6^{4-}$ band has its maximum (+0.30 V). However, this band decreases in intensity with further increase in potential, indicating a loss of some of the Fe(C $^{3-}$ species at high positive potentials. Electronic spectroscopy of solutions of $K_3Fe(CN)_6$ under these same conditions indicate that the $Fe(CN)_6^{3-}$ species is stable in bulk

solution. The disappearance of $Fe(CN)_6^{3-}$ can be most easily explained by adsorption onto the electrode at very positive potentials. There are two other bands in the spectrum, a peak at 2092 cm^{-1} and a shoulder at 2061 cm^{-1}.

The 2092 cm^{-1} band shifts in frequency with potential (by -100 cm^{-1}/V) and its intensity varies with potential in the opposite manner to the intensity of the 2114 cm^{-1} $Fe(CN)_6^{3-}$ band. The 2092 cm^{-1} band can therefore be assigned to the adsorption product of $Fe(CN)_6^{3-}$. The shoulder at 2061 cm^{-1} is at the same wavelength as adsorbed CN^- (this refers to a separate experiment in which previously adsorbed CN^- was displaced from the electrode by SO_4^{2-} as the potential was stepped from -0.20 V to +0.40 V). This band is evidence for surface decomposition of $Fe(CN)_6^{3-}$ upon adsorption.

The same experiment was performed on a solution containing $K_3Fe(CN)_6$ as the substrate instead of $K_4Fe(CN)_6$ (Figure 40). In this case, the base potential, to which the spectra were normalized to give $\Delta R/R$ values, was +0.4 V.

At this potential adsorbed $Fe(CN)_6^{3-}$ must be present. The band at 2114 cm^{-1}, corresponding to loss of $Fe(CN)_6^{3-}$ at the more negative potential, approaches a maximum intensity and remains constant. The $Fe(CN)_6^{4-}$ band at 2040 cm^{-1}, corresponding to production of that species, does the same. There is no evidence for the production of a new adsorbed species following the reduction of $Fe(CN)_6^{3-}$, nor desorption of the adsorbed species discussed above. This experiment suggests that the adsorption of $Fe(CN)_6^{3-}$ at high positive potentials is irreversible.

Further evidence for the irreversibility of the adsorption is provided by data from the difference spectra as a function of potential modulation using the usual pulse technique. With other experimental conditions the same as for above (i.e., using the substrate $K_4Fe(CN)_6$, and a base potential of -0.20 V), only the bands for removal of bulk $Fe(CN)_6^{4-}$ (2040 cm^{-1} and for

formation of bulk $(Fe(CN)_6^{3-}$ (2114 cm^{-1}) can be seen. Furthermore, the intensity of both bands decreases as the potential is made more positive than about +0.20 V. This effect is due to the depletion of electroactive species in the thin layer at high positive potentials and is evidence for irreversible adsorption onto the electrode at a given potential; the resulting signal-averaged coadded spectra would be expected to exhibit lower intensities than for a simple reversible charge transfer process, since a portion of the redox couple is removed from the thin layer. (It should be noted that the total amount of $Fe(CN)_6^{4-}$ in the thin layer initially is approximately the amount necessary to provide monolayer coverage, if all the material is adsorbed).

The above data suggests, then, that ferricyanide ion, $Fe(CN)_6^{3-}$, is strongly adsorbed at a smooth platinum electrode. The adsorption begins at about +0.25 V vs. SCE and increases in coverage with increasing positive potential (as can be seen from the decrease in the amount of electroactive species with potential in the thin layer). The initially adsorbed species partially dissociates to form an irreversibly adsorbed surface complex. The shift to lower wavenumber of the C ≡ N stretch band upon adsorption and the negative value of $d\bar{\nu}_{max}/dE$ indicate that the C ≡ N bonds are oriented parallel to the surface and are adsorbed through the π-system rather than through the nitrogen lone pair, (which would shift the C ≡ N stretch wavenumber positive on adsorption). The potential dependent shoulder (initially at 2061 cm^{-1}) appears to be due to an irreversibly adsorbed CN^- species. The adsorbate does not impede further oxidation of ferrocyanide, i.e., it supports further electron transfer from the metal to the remaining substrate in the solution.

If a deconvolution program is applied to the band at 2060 cm^{-1}, and the resulting integrated band intensity determinied, an estimate of the amount of adsorbed CN^- may be made. This is done by comparing this area with that

obtained for fully desorbing a known amount of CN^- electrochemically by replacement with SO_4^{2-} ion on the same electrode in thin layer cell. The results show that three CN^- ions per $Fe(CN)_6^{3-}$ ions are formed in the surface decomposition, leaving $[Fe(CN)_3]$ as the likely adsorbed species, in agreement with radiotracer experiments performed by Kaniewska (reported by Kawiak, et. al. (100)).

2.5.7. Phosphoric Acid Species

Habib and Bockris (103), utilizing the SNIFTIRS technique with a Digilab FT20E spectrometer system, have observed the potential dependent difference spectra of phosphosphoric acid solutions at a polycrystalline platinum electrode. At potentials between 0 and 800 mV (NHE) strong, potential dependent adsorption of phosphoric acid was observed via the intensity of the 1074 cm^{-1} P-O stretching mode. Perchlorate ion is drawn into the double layer by a mechanism similar to that described in Section 2.3.4. Coverage by the phosphoric acid species was shown to increase to a maximum at about 800 mV and then decrease, in accordance with radiotracer measurements. Work on the ionic contributions to the spectra is still in progress.

3.1. FUTURE DIRECTIONS

The field of infrared spectroelectrochemistry is in its infancy. The possibility of using FTIR instrumentation for the study of reaction dynamics via emission from the electrode surface is now being investigated. Time resolved techniques, traditionally reserved for the Raman experimentalists, is another area of great promise, again most easily effected by the use of rapid

scan interferometers. Ennancement of sensitivity so that catalytic activity at the 0.01 monolayer level can be observed is another goal that can be realized by the development of better instrumentation such as reproducible optical subtraction techniques, the use of cooled array detectors, and implementation of higher resolution A/D converters, just to mention a few. Extention of the techniques to the far-infrared will reveal details of the metal surface-adsorbate bond, as well as information on adsorbate-adsorbate interaction, adatom behavior, charge transport mechanisms through membranes and chemically modified electrodes, and other areas of fundamental importance.

An expansion of the experiments to include more work on well defined surfaces, such as single crystals, is imperative, and will undoubtedly provide more details on the exact orientations of adsorbates, and will provide a strong basis for treatment of spectra on the basis of two-dimensional lattice interactions with these adsorbates. The investigation of the effect of strong electric and magnetic fields on species at or near the interface will lead to further information regarding the structure and orientation of species, as well as the composition and potential structure of the electrical double layer.

Acknowledgements

S.P. gratefully acknowledges the support of the Office of Naval research, Washington, D.C. for most of this work. The importance of the contributions of the co-workers in these experiments (listed in the references) cannot be overemphasized.

References

1. Mark, H.B.; Pons, S. Anal. Chem. 38, 119 (1966).

2. Reed, A.H.; Yeager, E. Electrochim. Acta 15, 1345 (1970).

3. Tallant, D.; and Evans, D. Anal. Chem. 41, 835 (1969).

4. Fleischmann, M.; Hendra, P.J.; McQuillan, A.J. J. Chem. Soc. Chem. Comm. 80 (1973).

5. Fleischmann, M.; Hill, I.R. in R.K. Chang and T.E. Furtak (Eds.), Electrochemical Effects in Surface Enhanced Raman Scattering, Plenum Press, New York (1982).

6. Campion, A. paper presented at "Ellipsometry and Other Optical Methods for Surface and Thin Film Analysis", Paris, France, June 1983.

7. Fleischmann, M. paper presented at the 34th ISE meeting, Erlangen, West Germany, September 1983.

8. Pons, S.; Ph.D. Thesis, University of Southampton, 1979.

9. Bewick, A.; Robinson, J. J. Electroanal. Chem. 60, 163 (1975).

10. Bewick, A.; Robinson, J. Surf. Sci. 55, 349 (1976).

11. Adzic, R.; Cahan, B.D.; Yeager, E. J. Chem. Phys. 58 (1973) 1780.

12. Bewick, A.; Mellor, J.M.; Pons, S. Electrochim. Acta 25, 931 (1980).

13. See Pons, S.; Bewick, A. Naval Research Reviews, in press, and references therein.

14. See Bewick, A.; abstract Electrochem. Soc. Meeting, Montreal, 1982.

15. Golden, W.G.; Dunn, D.S.; Overend, J. J. Catal. 71, 395 (1981).

16. Golden, W.G.; Saperstein, D.; Severson, M.W.; Overend, J. J. Phys. Chem. 88, 874 (1984).

17. Russell, J.W.; Overend, J.; Scanlon, K.; Severson, M.; Bewick, A. J. Phys. Chem. 86, 3066 (1982); Russell, J.W.; Severson, M.; Scanlon, K.; Overend, J.; Bewick, A. J. Phys. Chem. 87, 293 (1983).

18. Golden, W.G.; Kunimatsu, K.; Seki, H. J. Phys. Chem. 88 1275 (1984).

19. Kunimatsu, K.; Seki, H.; Golden, W.G. J. Phys. Chem., in press.

20. Kunimatsu, K. J. Electroanal. Chem. 140, 205 (1982) and 145, 219 (1983).

21. Greenler, R.G. J. Chem. Phys. 44, 310 (1966).

22. S. Pons, J. Electroanal. Chem. 150, 495 (1983).

23. Bewick, A.; Kunimatsu, K.; Pons, S.; Russell, J.W. Electroanal. Chem., in press.

24. Devlin, J.P.; Consani, K. J. Phys. Chem. 85, 2597 (1981).

25. Pons, S.; Korzeniewski, C.; Bewick, A. J. Phys. Chem. in press.

26. Condon, E.V. Phys. Rev. 41, 759 (1932).

27. Crawford, M.F.; MacDonald, R.E. Can. J. Phys. 36, 1022 (1958).

28. Hauge, R.H.; Margrave, J.L.; Kaufman, J.W.; Rao, N.A.; Konarski, M.M.; Bell, J.P.; Billups, W.E. J. Chem. Soc. Chem. Commun. 1258 (1981).

29. Douglas, M.A.; Hauge, R.H.; Margrave, J.L. High Temp. Sci. 16 55 (1983).

30. Bradshaw, A.M.; Hoffman, T. Surf. Sci. 52, 449 (1975).

31. Golden, W.D.; Saperstein, D. J. Elev. Spectros. 30, 43 (1983).

32. Seki, H.; Kunimatsu, K.; Golden, W.G. Appl. Spectros. in press.

33. Hipps, K.W.; Crosby, G.A. J. Phys. Chem. 83, 555 (1979).

34. Hinds International, Inc., Portland, OR.

35. Bewick, A.; Russell, J.W. J. Electroanal. Chem. 132, 329 (1982).

36. Bewick, A.; Russell, J.W. J. Electroanal. Chem. 142, 337 (1982).

37. Capon, A.; Parsons, R. J. Electroanal. Chem. 44, 1 (1973).

38. McNicol, B.D. J. Electroanal. Chem. 118, 71 (1981).

39. Breiter, M.W. J. Electroanal. Chem. 14, 406 (1967), and 15, 221 (1967).

40. Biegler, T. Aust. J. Chem. 22, 1583 (1969).

41. Sobrowski, S.; and Wiecowski, A. J. Electroanal. Chem. 34, 185 (1972) and 63, 365 (1975).

42. Allen, G.C.; Tucker, P.M.; Capon, A. and Parsons, R. J. Electroanal. Chem. 50, 335 (1974).

43. Beden, B.; Lamy, C.; Bewick, A.; and Kunimatsu, K. J. Electroanal. Chem. 121, 343 (1981).

44. Beden, B.; Bewick, A.; and Lamy, C. J. Electroanal. Chem. 148, 147 (1983).

45. Bewick, A.; Kunimatsu, K.; Beden, B; Lamy C. 32nd ISE Meeting, Dubrovnik, Sept. 1981, Ext. Abstr. A28, Vol. 4, p. 92.

46. Bewick, A.; and Solomun, T. in preparation.

47. Sheppard, N.; and Nguyen, T.T. in Advances in Infrared and Raman Spectroscopy, (R.J.H. Clark and R.E. Hester, Eds.), Heyden, London, 1978, Vol. 5.

48. Beden, B.; Bewick, A.; Kunimatsu, K.; and Lamy, C. J. Electroanal. Chem. 142, 345 (1982).

49. Bewick, A.; and Solomun, T. J. Electroanal. Chem., in press.

50. Bewick, A. J. Electroanal. Chem., in press.

51. Bradshaw, A.M.; Hoffmann, F.M. Surf. Sci. 72, 513 (1978).

52. Bewick, A.; Beden, B.; Razaq, M.; and Weber, J. J. Electroanal. Chem. 139, 203 (1982).

53. Spasojevic, M.; Adzic, R.R.; and Despic, A.R. J. Electroanal. Chem. 109, 261 (1980).

54. Bewick, A. Symp. Chem. and Phys. of Electrocatalysis, The Electrochemical Society, San Francisco, May 1983.

55. Bewick, A.; and Solomun, T. in preparation.

56. Blyholder, G. J. Phys. Chem. 68, 2772 (1964).

57. Blyholder, G.; Sheets, R.W. J. Catal. 27, 301 (1972).

58. Hammakar, R.A.; Francis, S.A.; and Eischens, R.P. Spectrochim. Acta 21, 1295 (1965).

59. Scheffler, M. Surf. Sci. 81, 562 (1979).

60. Moskovitz, M.; and Hulse, J.E. Surf. Sci. 78, 397 (1978).

61. Crossley, A.; and King, D.A. Surf. Sci. 95, 131 (1980).

62. Bewick, A.; Razaq, M.; and Russell, J.W. Surf. Sci., in press.

63. Russell, J.W.; and Seversen, M.W. 188th Meeting Am. Chem. Soc., Coll 100, Philadelphia (1984).

64. Pons, S. Langmuir, in press.

65. Hubbard, A.T.; Stickney, J.; Soriaga, M.; Chia, V.; Rosasko, S.; Schardt, B.; Solomun, M.; Song, D.; White, J.; Wieckowski, A. J. Electroanal. Chem. 168, 43 (1984).

66. Bewick, A.; Hudec, J.; and Razaq, M., in preparation.

67. Bewick, A.; Gibilaro, C.; and Pons, S., in preparation.

68. Barclay, D.J. J. Electroanal. Chem. 19, 318 (1968). Barclay, D.J.; and Caja, J. Croatica Chem. Acta 43, 221 (1971).

69. Pons, S.; Davidson, T.; and Bewick, A. J. Electroanal. Chem. 140, 211 (1982).

70. Davidson, T.; Pons, S.; Bewick, A.; Schmidt, P.P. J. Electroanal. Chem. 125, 237 (1981).

71. Saumagne, P. Ph.D. Thesis, Université de Bordeaux, France, 1981.

72. Gentric, E. Ph.D. Thesis, Université de Bretagne Occidentale, France, 1972.

73. Saumagne, P.; and Josien, M.L. Bull. Soc. Chim. France, 813 (1958).

74. Pons, S.; Davidson, T.; and Bewick, A. J. Amer. Chem. Soc. 105, 1802 (1983).

75. Juchnovski, I. Spectrochim. Acta 29, 1273 (1973).

76. Aleksandrov, I.V.; Bobovich, Y.S.; Maslovad, V.G. and Sidorov, A.N. Opt. Spectros. 35, 154 (1973).

77. Pons, S.; Smith, J.J. in preparation.

78. Pons group and University of Utah.

79. Pons, S.; Khoo, S.B.; Bewick, A; Datta, M.; Smith, J.J.; Hinman, A.S.; and Zachmann, G. J. Phys. Chem. 88, 3575 (1984).

80. a. Jeanmaire, D.L.; Suchanski, M.R.; Van Duyne, R.P. J. Amer. Chem. Soc. 97, 1699 (1975); b. Pemberton, J.E.; and Buck, R.P. Appl. Spectros. 35, 571 (1981); c. Devlin, J.P., private communication.

81. a. Khatkale, M.S.; Devlin, J.P. J. Phys. Chem. 83, 1637 (1979); b. Moore, J.C.; Smith, D.; Youhne, Y.; and Devlin, J.P., ibid, 75, 325 (1971); c. Hinkel, J.J.; and Devlin, J.P. J. Chem. Phys., 58, 4750 (1973) and references therein; d. Hemminger, John; private communication.

82. Bewick, A.; Razaq, M.; Russell, J.W.; and Solomun, T., in preparation.

83. Bewick, A.; Dubetz, T.; Pons, S.; and Razaq, M., in preparation.

84. Cooney, R.P.; Reid, E.S.; Fleischmann, M.; and Hendra, P.J. J. Chem. Soc. Faraday I, 73, 1691 (1977). Gold, H.S.; and Buck, R.P. J. Raman Spectroscopy 8, 323 (1979). Wetzel, H.; Gerischer, H.; and Pettinger, B. Chem. Phys. Letts. 80, 159 (1981).

85. Bewick, A.; Gibi -o, C., in preparation.

86. Otto, A. Surf. Sci. 75, L392 (1978).

87. Furtak, T.E. Solid State Commun. 28, 903 (1978).

88. Dornhaus, R.; Long, M.B.; Benner, R.E.; and Chang, R.K. Surf. Sci. 93, 240 (1980).

89. Billmann, J.; Kovacs, G.; and Otto, A. Surf. Sci. 92, 153 (1980).

90. Benner, R.E.; Dornhaus, R.; Chang, R.K.; and Lanbe, B.L. Surf. Sci. 101, 341 (1980).

91. Otto, A. Surf. Sci. 92, 145 (1980).

92. Timper, J.; Billman, J.; Otto, A.; and Pockrand, I.B. Surface Sci. 101, 348 (1980).

93. Furtak, T.E.; Trott, G.; and Loo, B.H. Surface Sci. 101, 374 (1980).

94. Loo, B.H.; and Furtak, T.E. Chem. Phys. Letters 71, 68 (1980).

95. Genack, A.Z.; Weitz, D.A.; and Granila, T.J. Surface Sci. 101, 381 (1980).

96. Kotz, R.; and Yeager, E. J. Electroanal. Chem. 123, 335 (1981).

97. Fleischmann, M.; Hill, I.R.; and Pemble, M.E. J. Electroanal. Chem. 136, 361 (1982).

98. Kuta, J.; and Yeager, E. J. Electroanal. Chem. 59, 110 (1975).

99. Peter, L.M.; Durr, W.; Bindra, P.; and Gerischer, H. J. Electroanal. Chem. 71, 31 (1976).

100. Kawiak, J.; Jedral, T.; Galus, Z. J. Electroanal. Chem. 145, 163 (1983).

101. Wieckowski, A.; and Szklarcyk, M. J. Electroanal. Chem. 142, 157 (1982).

102. Pons, S.; Datta, M.; and Hinman, S., in preparation.

103. Habib, M.A.; Bockris, J.O.'M. J. Electrochem. Soc. 130, 2510, 1983.

Figure 1 Phase shift for radiation reflected from a metal surface as a function of angle of incidence. E_3 represents radiation polarized perpendicular to the plane of incidence and E_p represents radiation polarized parallel to the plane of incidence.

Figure 2 Variation of the standing-wave fields at a highly reflecting surface (D = 3.0 and K = 30) in contact with a transparent phase (n_2 = 1.0) as a function of the angle of incidence, ϕ. $\langle E^2_s \rangle / \langle E^2_i \rangle$ is the ratio of the mean square electric field strength for the standing wave and the incident wave.

Figure 3 A. Illustration of formation of surface normal dipole derivative with respect to stretch of bond parallel to surface. The effect of bonding this molecule to a surface atom is to reduce the symmetry of the adsorbate to C_{2v}. Solid line-compressed bond and surface normal dipole. Dotted line-extended bond and surface normal dipole.

B. Possible orientations for CO and N_2 adsorbed at a surface.

Figure 4 The design of the spectroelectrochemical cell used for the EMIRS and SNIFTIRS measurements.

Figure 5 Reflectance apparatus for the SNIFTIRS technique.

Figure 6 EMIRS spectrum from a polycrystalline Rhodium electrode in 0.5 M $HClO_4$ and 0.1 M HCHo. Modulation + 0.5 V to + 0.45 V (NHE) at 8.4 Hz.

Figure 7 Spectra from a polycrystalline platinum electrode in 0.5 M $HClO_4$ saturated with CO: (a) IRRAS spectra at +650, +450, +250 and +150 mV (from left to right) us NHE, (b) IRRAS difference spectrum constructed by subtraction of +50 mV spectrum from +450 mV spectrum in (a), (c) EMIRS spectrum for modulation +50 mV to +450 mV.

Figure 8 Difference spectra from a palladium electrode in 1 M H_2SO_4 containing CO: electrode coverages by adsorbed CO: (a) 0.34, (b) 0.39, (c) 0.41, (d) 0.41, (e) 0.42, (f) 0.48 and (g) 0.64.

Figure 9 Band position as a function of coverage, Θ, for (a) the major band in the EMIRS spectra of Figure 8 and (b) the band reported in Reference 51 for Pd (111)/CO in the gas phase.

Figure 10 Difference spectra from a polycrystalline platinum electrode in spectra from 1 M H_2SO_4 saturated with CO_2. Modulation at 8.5 Hz (a) +0.25 V to +0.55 V, (b) +0.15 V to +0.55 V and (c) +0.05 V to +0.45 V vs. NHE.

Figure 11 Difference spectra from a platinum electrode in 0.5 $HClO_4$ and 0.1 M HCHO for two ranges of potential: 0 to 250 mV (left hand side); and 0 to 400 mV (right hand side) in the absence (a) and in the presence (b) of a submonolayer amount of electrodeposited lead.

Figure 12 Difference spectra from a polycrystalline platinum electrode in 1 M H_2SO_4 saturated with $C_{12}O/C_{13}O$, the isotopic ratio changing progressively from 100% C_{13} in (a) to 100% C_{12} in (f).

Figure 13 Difference spectra of samples containing ^{12}CO and ^{13}CO in 1 M H_2SO_4 at a Pt electrode. Modulation potentials all 50 to 450 mV vs NHE. A-C high coverage, D-F low coverage. Percent ^{13}CO: 30% (A and D); 50% (B and E); 90% (C and F). Intensity scale for low coverage, D through F, is twice as sensitive as A through C.

Figure 14 SNIFTIRS difference spectrum of p-difluorobenzene at a platinum electrode in 1.0 M $HClO_4$. Potential modulation limits are from +0.200 to +0.400 V vs NHE.

Figure 15 SNIFTIRS difference spectra for meta- and ortho-difluorobenzene. Parameters same as Figure 14.

Figure 16 SNIFTIRS difference spectra of the B_{3u} ring bending mode of p-difluorobenzene as a function of modulation potential. Other parameters same as Figure 14.

Figure 17 SNIFTIRS difference spectra of the B_{3u} ring bending mode of p-difluorobenzene between +0.200 and +0.400 mV vs. NHE as a function of solution concentration at 281 K.

Figure 18 Difference spectra of benzonitrile in the CN stretch region. Gold electrode in 1.0 M H_2SO_4 and 0.02 M benzonitrile. Potential modulation regions are indicated on the appropriate spectrum. Modulation frequency was 8.5 Hz.

Figure 19 Difference spectrum of benzonitrile in the ring mode region. Potential modulation limits were 0.00 V and 1.10 V vs. NHE. Other parameters same as Figure 18.

Figure 20 Differential double layer capacity vs. applied potential relations for a polycrystalline gold electrode in (a) 1 M H_2SO_4 and (b) 1 M H_2SO_4 and 0.05 M acrylonitrile; ac modulation 5 mV p-p at 8.5 Hz superimposed on a potential ramp (0.01 $V\text{-}S^{-1}$).

Figure 21 EMIRS difference spectrum from a gold electrode in 1 M H_2SO_4 and 0.05 M acrylonitrile. Modulation frequency at 8.5 Hz from -0.195 V to +0.350 V.

Figure 23 Potential dependence of the frequency position of the CN stretch mode of adsorbed acrylonitrile.

Figure 24 SNIFTIRS difference spectra at a platinum electrode in 0.1 M tetra-n-butylammonium tetrafluoroborate (TBAF) in nominally dry acetonitrile as a function of potential vs. Ag/Ag^+ (0.01 M $AgNO_3$ and 0.1 M TBAF in acetonitrile).

Figure 25 Same as Figure 24 with 0.10 M H_2O.

Figure 26 SNIFTIRS difference spectra at a platinum electrode in 0.1 M $LiClO_4$ in nominally dry acetonitrile. Other parameters same as Figure 24.

Figure 27 Same as Figure 26 with 0.10 M H_2O.

Figure 28 A. Transmission spectrum of benzophenone.

B. The SNIFTIRS difference spectrum of benzophenone reduction to the ketyl anion radical.

Figure 29 A. Transmission spectrum of anthracene, KBr pellet.

B. SNIFTIRS difference spectrum for anthracene reduction to the anion radical. Platinum electrode in 0.1 M TBAF in acetonitrile. Modulation potential -1.50 V to -2.50 V vs. Ag/Ag^+ reference.

Figure 30 SNIFTIRS difference spectrum for 2,6-di-t-butyl-4-phenylaniline oxidation to the cation radical. Platinum electrode in 0.1 M TBAF in acetonitrile. Modulation potential 0.0 V to +0.800 V vs. Ag/Ag^+ reference.

Figure 31 Cyclic voltammetry of TCNE in acetonitrile: (a) 0.1 M TBAF; (b) 0.1 M $LiClO_4$. ν = 50 mV-s^{-1}, platinum electrode.

Figure 32 IR spectra for various states of TCNE in the CN stretch region. (a) KBr pellet; (b) Nujol mull; (c) in acetonitrile; (d) TCNE anion radical in acetonitrile.

Figure 33 Surface SNIFTIRS spectrum for tetracyanoethylene reduction in the first voltammetric wave. Solution thickness approximately 1 μm; (a) in 0.1 M tetrabutylammonium tetrafluoroborate; (b) in 0.1 M lithium perchlorate. Potential modulation limits + 0.5 to - 0.5 V vs. Ag/Ag^+ reference.

Figure 34 Surface SNIFTIRS spectra for tetracyanoethylene reduction in the first voltammetric wave as a function of bulk substrate concentration: (a) top to bottom 1.0, 2.0, 5.0 mM. TBAF is supporting electrolyte. Solution thickness approximately 1 μm.

Figure 35 Comparisons of SNIFTIRS spectra for TCNE reduction as a function of radiation polarization: (a) pure perpendicular with respect to surface; (b) mixed p- and s-polarization with respect to surface.

Figure 36 EMIRS difference spectra from a polycrystalline gold electrode in 1 M H_2SO_4. Modulation potentials (NHE) are: (a) + 50 mV to +500 mV, (b) + 50 mV to +700 mV, (c) + 50 mV to +1150 mV, (d) +650 mV to 1250 mV; all at 8.5 Hz modulation frequency.

Figure 37 SNIFTIRS difference spectra from a platinum electrode in 1 M NaF and 0.01 M KSCN. Measured at +600 mV (Lowest trace). -650 mV, -700 mV, -800 mV, ±900° mV and +100 mV (top trace) against a fixed base potential of -400 mV vs. SCE reference.

Figure 38 EMIRS difference spectra for a polycrystalline gold electrode in 1 M Na_2SO_4 and 5 mM KSCN. Modulation frequency is 8.5 Hz and potentials are from -1.00 V (NHE) to (a) -0.50 V, (b) -0.20 V, (c) +0.20 V, (d) +0.60 V and (e) +0.75 V.

Figure 39 Surface SNIFTIRS spectra for $Fe(CN)_6^{4-}$ oxidation at a platinum electrode using the staircase mode. Lowest trace takes a 0.00 V, the next at +0.10 V then at 0.05 V increments up to 0.60 V.

Figure 40 SNIFTIRS spectra at a platinum electrode as a function of potential using the staircase method for the reduction of $Fe(CN)_6^{3-}$. Base potential +0.40 V in each case; reduction potentials, from top to bottom, +0.30 V, +0.25 V, +0.20 V, +0.15 V, +0.10 V, +0.05 V, 0.00 V, -0.10 V, -0.20 V. vs. SCE reference.

END

DATE

FILMED

6-1988

DTIC